Karlsruhe Institute of Technology

Evaluation of Different Strategies for Goal-Oriented Adaptivity in CFD

Part I: The Stationary Case

Martin Baumann
Vincent Heuveline

No. 2010-05

Preprint Series of the Engineering Mathematics and Computing Lab (EMCL)

KIT – University of the State of Baden-Wuerttemberg and
National Research Center of the Helmholtz Association

www.emcl.kit.edu

Preprint Series of the Engineering Mathematics and Computing Lab (EMCL)
ISSN 2191–0693
No. 2010-05

Impressum

Karlsruhe Institute of Technology (KIT)
Engineering Mathematics and Computing Lab (EMCL)

Fritz-Erler-Str. 23, building 01.86
76133 Karlsruhe
Germany

KIT – University of the State of Baden Wuerttemberg and
National Laboratory of the Helmholtz Association

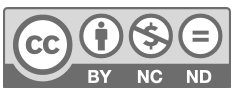

Evaluation of Different Strategies for Goal Oriented Adaptivity in CFD – Part I: The Stationary Case

Martin Baumann and Vincent Heuveline

Karlsruhe Institute of Technology (KIT)

Engineering Mathematics and Computing Lab (EMCL)

Fritz-Erler-Str. 23

76133 Karlsruhe, Germany

martin.baumann@kit.edu, vincent.heuveline@kit.edu

Abstract

Many goal oriented adaptive methods are based on a characterization of the error with respect to a user-defined functional. This error can be quantified by means of a dual solution, but depends on unknown quantities. Different strategies exist to recover the sensitivity information that go along with the approximation of these unknowns. In this paper a systematical comparison of such evaluation strategies with respect to the corresponding efficiency and reliability of the computable error estimators is presented. The investigation is based on two CFD scenarios with analytically known exact solution of the stationary incompressible Navier-Stokes equations.

1 Introduction

Many flow problems are influenced by physical structures and processes on a wide range of scales. For the numerical modelling and simulation of such phenomena, very high resolution of the mesh is needed to resolve the fine structures, which can yield memory- and CPU-intensive calculations. For many applications not all of the existing processes can be resolved accurately even on today's high-performance computers. Adaptive methods based on a posteriori error estimators [AO00, Ver96, EEHJ95] can be used to improve the quality of the mesh or the models to achieve higher accuracy and computational efficiency. In particular, goal oriented adaptive methods have been developed in the last decade (see [BHR02, BR03, BE03, BR06, HW06, SV07] and references therein), allowing the determination of those features that should be resolved in order to compute a given goal functional accurately.

In this work the Dual Weighted Residual (DWR) [EEHJ95, BR03] method is investigated in more detail. Although the DWR method is already widely established in many fields of application [BR99, BEG03, Ste03, HR06, Har08], the use of this technique in operational software codes is still rare. One of the main reasons is the highly abstract character of this approach. The underlying mathematical principles, which are meanwhile well understood, admit a variety of different strategies to extract and use the sensitivity information in an adequate way. It turns out that the quality of these techniques and their practicability in the framework of complex and large problems depend on the deployment strategy the choice of which requires empirical knowledge in addition to mathematical arguments. In that context the tradeoff between computational cost and accuracy which needs to be adressed in CFD is still a challenge, where the idiom "the devil is in the details" applies to the full extent. The goal of this paper is to compare in a systematic way different deployment strategies of the DWR method for stationary flow problems modelled with the Navier-Stokes equations.

The outline of this paper is as follows: In Section 2 three variants of an a posteriori error estimator that are the basis of the considered goal oriented methods are described in an abstract setting. In Section 3 error estimators are derived for the Navier-Stokes equations, including the localized error indicators that can be used to control the mesh adaptation. In Section 4 different strategies to compute these error estimators are presented, which are applied systematically to two scenarios with analytically known exact solutions of the Navier Stokes equations for several goal functionals. The results of the adaptive numerical simulations are described in Section 5. A short summary and outlook is given in Section 6.

2 Goal oriented error estimation

Based on the derivation proposed in [BR03], we outline the definition of the considered a posteriori error estimator for an abstract problem. Let $A : V \times V \to \mathbb{R}$ be a semi-linear functional, that might be non-linear in the first parameter, and let $F : V \to \mathbb{R}$ be a linear functional, defined on a Hilbert space V. Furthermore, assume the existence of directional derivatives of A up to the order of three. Consider the variational problem:

Find $u \in V$ such that

$$A(u;\varphi) = F(\varphi), \quad \forall \varphi \in V, \tag{1}$$

and suppose the existence of a unique solution. For a given *goal functional* $J : V \to \mathbb{R}$, let $J(u)$ denote the quantity of interest, where u denotes the solution of (1). Further define the corresponding *dual* or *adjoint* problem:

Find $z \in V$ such that

$$\nabla_u A(u;z)(\varphi) = \nabla_u J(u)(\varphi), \quad \forall \varphi \in V, \tag{2}$$

where u is again the solution of (1). For a discrete conformal finite element space $V_h \subset V$ Galerkin approximations for the primal and dual problem are given by:

Find $(u_h, z_h) \in V_h \times V_h$, such that

$$\begin{aligned} A(u_h;\varphi_h) &= F(\varphi_h), \qquad \forall \varphi_h \in V_h, & (3)\\ \nabla_u A(u_h;z_h)(\varphi_h) &= \nabla_u J(u_h)(\varphi_h), \quad \forall \varphi_h \in V_h. & (4) \end{aligned}$$

The error in the goal functional $J(u) - J(u_h)$ can be approximated in terms of the solution (u, z) of the variational problems (1) and (2) and the Galerkin approximation (u_h, z_h) using one of the following three equalities [BR03]:

$$\begin{aligned} J(u) - J(u_h) &= \rho(u_h; z - \varphi_h) + \mathcal{R}_2 \quad \forall \varphi_h \in V_h,\\ J(u) - J(u_h) &= \rho^*_{u_h}(z_h; u - \psi_h) + \tilde{\mathcal{R}}_2 \quad \forall \psi_h \in V_h,\\ J(u) - J(u_h) &= \frac{1}{2}\left(\rho(u_h; z - \varphi_h) + \rho^*_{u_h}(z_h; u - \psi_h)\right) + \mathcal{R}_3 \quad \forall \varphi_h, \psi_h \in V_h, \end{aligned} \tag{5}$$

where $\rho(u_h;\cdot)$ and $\rho^*_{u_h}(z_h;\cdot)$ denote the residuals of the primal and the dual problems, respectively:

$$\begin{aligned} \rho(u_h;\cdot) &:= F(\cdot) - A(u_h;\cdot) \quad \text{in } V,\\ \rho^*_{u_h}(z_h;\cdot) &:= \nabla_u J(u_h)(\cdot) - \nabla_u A(u_h;z_h)(\cdot) \quad \text{in } V. \end{aligned}$$

The remainder terms $\mathcal{R}_2$ and $\tilde{\mathcal{R}}_2$ are quadratic and $\mathcal{R}_3$ is cubic in the errors $e := u - u_h$ and $e^* := z - z_h$. Replacing the unknown solutions u and z by approximations $\tilde{u} \approx u$ and $\tilde{z} \approx z$ in the residual expressions (5) and neglecting the remainder terms yields three a posteriori error representations for the error $J(u) - J(u_h)$:

$$\begin{aligned} J(u) - J(u_h) &\approx E_P(u_h) := \rho(u_h; \tilde{z} - \varphi_h),\\ J(u) - J(u_h) &\approx E_D(u_h) := \rho^*_{u_h}(z_h; \tilde{u} - \psi_h),\\ J(u) - J(u_h) &\approx E_{PD}(u_h) := \frac{1}{2}\rho(u_h; \tilde{z} - \varphi_h) + \frac{1}{2}\rho^*_{u_h}(z_h; \tilde{u} - \psi_h) \end{aligned} \tag{6}$$

for all $\varphi_h, \psi_h \in V_h$. Using these a posteriori error representations, the approximate value $J(u_h)$ of $J(u)$ can be postprocessed and expressed by

$$\tilde{J}_P(u_h) := J(u_h) + E_P(u_h) \tag{7}$$

and $\tilde{J}_D$ and $\tilde{J}_{PD}$ analogously. Until now, the choice of the discrete functions φ_h and ψ_h was not important since it does not influence the value of the error representations (6) due to the Galerkin orthogonality. To derive the local contributions of each cell to the total error in J, the discrete functions are chosen by a suitable interpolation ($I_h : V \to V_h$):

$$\varphi_h := I_h(\tilde{z}), \quad \psi_h := I_h(\tilde{\varphi}).$$

Each of the error representations (6) can be written as a sum over all cells $K \in \mathcal{T}_h$ of the discretized domain $\Omega = \bigcup_{K \in \mathcal{T}_h} K$, where $\mathcal{T}_h$ is the triangulation. Extracting the norms of the

cell-wise contributions, by the triangle inequality the a posteriori error estimator is given in terms of so-called *error indicators* $\eta_K, \eta_K^* > 0$ by (E_D and E_{PD} analogously):

$$\eta_P(u_h) := \sum_{K \in \mathcal{T}_h} \eta_K, \quad \eta_D(u_h) := \sum_{K \in \mathcal{T}_h} \eta_K^*, \quad \eta_{PD}(u_h) := \sum_{K \in \mathcal{T}_h} \frac{1}{2}(\eta_K + \eta_K^*),$$

where $\eta_K \geq 0$ and $\eta_K^* \geq 0$ represent the contributions of cell $K \in \mathcal{T}_h$ to the error in J.

3 Error estimators for the Navier-Stokes equations

To derive goal oriented error estimators and local indicators for the Navier-Stokes equations, the residual operators of the corresponding primal and dual problem must be applied to the abstract framework described in Section 2. Let $\Omega \subseteq \mathbb{R}^d$, $d \in \{2, 3\}$ be a closed domain with sufficiently smooth boundary Γ, and let v and p denote the velocity field and the pressure distribution, respectively. Assuming for simplicity Dirichlet boundary conditions for the velocity field, the incompressible stationary Navier-Stokes equations have the following form:

$$-\nu \Delta v + (v \cdot \nabla) v + \frac{1}{\rho} \nabla p = f \quad \text{in } \Omega, \tag{8}$$

$$\nabla \cdot v = 0 \quad \text{in } \Omega, \tag{9}$$

$$v = v_D \quad \text{on } \Gamma, \tag{10}$$

$$\int_\Omega p = 0. \tag{11}$$

The function f denotes a volume force, the parameter $\nu > 0$ the kinematic viscosity and $\rho > 0$ the density of the fluid. A variational formulation of the **primal problem** is given by (see e.g. [Gal98]):

Find $(v, p) \in V_1^{(P)} \times V_2^{(P)}$ such that

$$((v \cdot \nabla) v, \varphi)_\Omega - \frac{1}{\rho}(p, \nabla \cdot \varphi)_\Omega + \nu (\nabla v, \nabla \varphi)_\Omega + (\nabla \cdot v, \psi)_\Omega = (f, \varphi)_\Omega \tag{12}$$

for all $(\varphi, \psi) \in W_1^{(P)} \times W_2^{(P)}$.

where $V_1^{(P)} := \{v \in H^1(\Omega)^d : v = v_D \text{ on } \Gamma\}$, $V_2^{(P)} := \{p \in L^2(\Omega) : \int_\Omega p \, dx = 0\}$, $W_1^{(P)} := \{v \in H^1(\Omega)^d : v = 0 \text{ on } \Gamma\}$ and $W_2^{(P)} := L^2(\Omega)$. The inner product in $L^2(\Omega)$ is denoted by $(a, b)_\Omega := \int_\Omega a \cdot b \, dx$. Given a goal functional $J : H^1(\Omega)^d \to \mathbb{R}$, the variational formulation of the corresponding **dual problem** described abstractly in Equation (2) is given by:

Find $(z, q) \in V_1^{(D)} \times V_2^{(D)}$ such that

$$((\varphi \cdot \nabla) v + (v \cdot \nabla) \varphi, z)_\Omega - \frac{1}{\rho}(\psi, \nabla \cdot z)_\Omega + \nu (\nabla \varphi, \nabla z)_\Omega + (\nabla \cdot \varphi, q)_\Omega = \nabla J(v, p)(\varphi, \psi) \tag{13}$$

for all $(\varphi, \psi) \in W_1^{(D)} \times W_2^{(D)}$.

Here v denotes the velocity component of the solution of (12). The spaces are defined as $V_1^{(D)} := \{v \in H^1(\Omega)^d : v = 0 \text{ on } \Gamma\}$, $V_2^{(D)} := \{p \in L^2(\Omega) : \int_\Omega p \, dx = 0\}$ and $W_1^{(P)} := \{v \in H^1(\Omega)^{(D)} :$

$v = 0 \text{ on } \Gamma\}$, $W_2^{(P)} := L^2(\Omega)$. For Galerkin approximations, conforming finite-dimensional spaces $V_{i,h}^{(P)} \subseteq V_i^{(P)}$, $V_{i,h}^{(D)} \subseteq V_i^{(D)}$, $W_{i,h}^{(P)} \subseteq W_i^{(P)}$ and $W_{i,h}^{(D)} \subseteq W_i^{(D)}$ $(i = 1, 2)$ that fulfill the Ladyschenskaja-Babuška-Brezzi (LBB) condition [Bre74] are chosen. For approximate solutions $(v_h, p_h, z_h, q_h) \in V_1^{(P)} \times V_2^{(P)} \times V_1^{(D)} \times V_2^{(D)}$ the error representations (6) have the form

$$\begin{aligned} E_P(v_h, p_h) &= \rho\left(v_h, p_h; \tilde{z} - I_h(\tilde{z}), \tilde{q} - I_h(\tilde{q})\right) \\ E_D(v_h, p_h) &= \rho^*_{(v_h, p_h)}\left(z_h, q_h; \tilde{v} - I_h(\tilde{p}), \tilde{v} - I_h(\tilde{p})\right) \\ E_{PD}(v_h, p_h) &= \frac{1}{2} E_P(v_h, p_h) + \frac{1}{2} E_D(v_h, p_h) \end{aligned} \tag{14}$$

As already mentioned in Section 2, the functions $\tilde{v} \approx v$, $\tilde{p} \approx p$, $\tilde{z} \approx z$ and $\tilde{q} \approx q$ denote some approximations of the exact solutions. Several strategies to compute these approximations will be specified in Section 4. Introducing for brevity the quantities $Z := \tilde{z} - I_h(\tilde{z})$ and $Q := \tilde{q} - I_h(\tilde{q})$, the contribution to the primal residual from a cell K is given by:

$$\begin{aligned} \rho_K &:= (f, Z)_K - ((v_h \cdot \nabla) v_h, Z)_K + \frac{1}{\rho}(p_h, \nabla \cdot Z)_K - \nu(\nabla v_h, \nabla Z)_K - (\nabla \cdot v_h, Q)_K \\ &= (f - (v_h \cdot \nabla) v_h - \frac{1}{\rho}\nabla p_h + \nu \Delta v_h, Z)_K + (\nabla \cdot v_h, Q)_K + (-\nu \partial_n v_h + \frac{1}{\rho} p_h n, Z)_{\partial K}. \end{aligned}$$

On the boundary $\gamma := \partial K' \cap \partial \hat{K}$ between each pair of two neighboring cells K' and $\hat{K}$ there are two contributions to the residual given by the following two integrals over γ:

$$(-\nu \partial_{n'} v_h' + \frac{1}{\rho} p_h' n', Z')_\gamma \quad \text{and} \quad (-\nu \partial_{\hat{n}} \hat{v}_h + \frac{1}{\rho} \hat{p}_h \hat{n}, \hat{Z})_\gamma,$$

where w' and $\hat{w}$ denotes the values of w on the cells K' and $\hat{K}$, respectively. Since Z is a globally continuous functions, $Z := Z' = \hat{Z}$ holds on γ. Furthermore, the normal unit vectors are antiparallel, i.e. $n := n' = -\hat{n}$ so that the residual contribution corresponding to γ is given by

$$(-\nu \partial_{n'} v_h' + \frac{1}{\rho} p_h' n', Z')_\gamma + (-\nu \partial_{\hat{n}} \hat{v}_h + \frac{1}{\rho} \hat{p}_h \hat{n}, \hat{Z})_\gamma = -\nu(\underbrace{\partial_n v_h' - \partial_n \hat{v}_h}_{=:[\partial_n v_h]}, Z)_\gamma + \frac{1}{\rho}((\underbrace{p_h' - \hat{p}_h}_{=:[p_h]})n, Z)_\gamma, \tag{15}$$

where $[\partial_n v_h]$ denotes the jump of the normal derivative and $[p_h]$ the jump of the pressure at the common cell boundary. For cell K and cell boundary γ, we can introduce the cell residual $resC$ and the boundary residual $resB$ defined by:

$$\begin{aligned} resC_{|K} &:= f - (v_h \cdot \nabla) v_h - \frac{1}{\rho}\nabla p_h + \nu \Delta v_h, \\ resB_{|\gamma} &:= \begin{cases} -\frac{1}{2}\nu[\partial_n v_h] + \frac{1}{2\rho}[p_h] n & \text{, if } \gamma \text{ is an inter-cell boundary} \\ -\nu \partial_n v_h + \frac{1}{\rho} p_h n & \text{, if } \gamma \subset \partial\Omega. \end{cases} \end{aligned}$$

The contribution of cell $K \in \mathcal{T}_h$ to the primal residual can be written as

$$\rho_K := (resC, Z)_K + (\nabla \cdot v_h, Q)_K + (resB, Z)_{\partial K}. \tag{16}$$

To describe the contribution of each cell to the dual residual, the goal functional $J(v, p)$ is assumed to be of the form

$$J(v, p) := (j^{(v)}, v)_\Omega + (j^{(p)}, p)_\Omega,$$

where $j^{(v)} \in L^2(\Omega)^d$ and $j^{(p)} \in L^2(\Omega)$. Introducing the quantities $V := \tilde{v} - I_h(\tilde{v})$ and $P := \tilde{p} - I_h(\tilde{p})$ for clarity, the contribution of cell $K \in \mathcal{T}_h$ to the dual residual is given by:

$$\begin{aligned}\rho_K^* &:= (j^{(v)}, V)_{|K} + (j^{(p)}, P)_{|K} \\ &\quad - ((V \cdot \nabla)v_h + (v_h \cdot \nabla)V, z_h)_K + \frac{1}{\rho}(P, \nabla \cdot z_h)_K - \nu(\nabla V, \nabla z_h)_K - (\nabla \cdot V, q_h)_K \\ &= (j^{(v)}, V)_{|K} + (j^{(p)}, P)_{|K} - ((\nabla v_h)^T z_h - (v_h \cdot \nabla)z_h - (\nabla \cdot v_h)z_h - \nabla q_h - \nu \Delta z_h, V)_K \\ &\quad + \frac{1}{\rho}(\nabla \cdot z_h, P)_K - ((v_h \cdot n) \cdot z_h + \nu \partial_n z_h + q_h n, V)_{\partial K}.\end{aligned}$$

The contribution corresponding to cell K and cell boundary γ to the dual residual is denoted by the dual cell residual $resC^*$ and the dual boundary residual $resB^*$:

$$\begin{aligned}resC^*_{|K} &:= j^{(v)} - (\nabla v_h)^T z_h + (v_h \cdot \nabla)z_h + (\nabla \cdot v_h)z_h + \nabla q_h + \nu \Delta z_h, \\ resB^*_{|\gamma} &:= \begin{cases} -\frac{1}{2}\nu[\partial_n z_h] - \frac{1}{2}[q_h]n & \text{, if } \gamma \text{ is an inter-cell boundary} \\ -(v_h \cdot n)z_h - \nu \partial_n z_h - q_h n & \text{, if } \gamma \subset \partial\Omega. \end{cases}\end{aligned}$$

On inter-cell boundaries the term $-(v_h \cdot n)z_h$ is zero, since v_h and z_h are globally continuous. The contribution of cell $K \in \mathcal{T}_h$ to the dual residual can be written compactly as

$$\rho_K^* := (resC^*, V)_K + (j^{(p)} + \frac{1}{\rho}\nabla \cdot z_h, P)_K + (resB^*, V)_{\partial K}.$$

The computable a posteriori error representations defined via the cell-wise contributions for the three variants are

$$E_P(u_h) := \left| \sum_{K \in \mathcal{T}_h} \rho_K \right|, \quad E_D(u_h) := \left| \sum_{K \in \mathcal{T}_h} \rho_K^* \right|, \quad E_{PD}(u_h) := \left| \frac{1}{2} \sum_{K \in \mathcal{T}_h} \rho_K + \rho_K^* \right|. \tag{17}$$

The corresponding a posteriori error estimators defined in terms of error indicators are

$$\eta_P(u_h) := \sum_{K \in \mathcal{T}_h} |\rho_K|, \quad \eta_D(u_h) := \sum_{K \in \mathcal{T}_h} |\rho_K^*|, \quad \eta_{PD}(u_h) := \sum_{K \in \mathcal{T}_h} \frac{1}{2}|\rho_K + \rho_K^*|, \tag{18}$$

where the cell-wise error indicators are defined as $\eta_K := \frac{1}{2}|\rho_K|$ and $\eta_K^* := |\rho_K^*|$.

4 Strategies of evaluation

The a posteriori error representations (17), error indicators and related error estimators (18) require the evaluation of residual expressions $\rho(u_h; \tilde{z} - I_h(\tilde{z}))$ and $\rho^*_{u_h}(z_h; \tilde{u} - I_h(\tilde{u}))$, where u_h and z_h denote Galerkin approximations characterized by (3) and (4). $I_h : V \to V_h$ denotes the nodal interpolation operator. $\tilde{u}$ and $\tilde{z}$ represent the exact solutions of the primal and dual problems (1) and (2), which are unknown in general. The question is how to calculate these approximations $\tilde{u}$ and $\tilde{z}$ to get reliable estimates without increasing computational cost in an intractable way. To the opinion of the authors, this key issue represents the true challenge of using the DWR method in CFD. In the following three strategies of evaluating the error estimators, i.e. the needed approximations, are investigated.

4.1 Higher-order finite element solution

Let $V_h \subset V$ denote the finite element space corresponding to the Galerkin approximations u_h and z_h. The solutions $u, z \in V$ are replaced by finite element solutions $\hat{u}_h, \hat{z}_h \in \hat{V}_h$, where $\hat{V}_h$ is a finite element space of higher-order ($V_h \subset \hat{V}_h$). The residuals that need to be evaluated for the a posteriori error representation (17) and error indicators (18) are

$$\rho(u_h; \hat{z}_h - I_h(\hat{z}_h)), \quad \rho^*_{u_h}(z_h; \hat{u}_h - I_h(\hat{u}_h)).$$

This strategy leads to accurate approximations of the unknown quantities in the error representations, but the related computational effort is considerably high. A drawback is that although higher-order approximations of the primal and dual solutions are calculated, still the estimations characterize the solution of the lower-order approximation u_h only.

4.2 Block strategy

The block strategy represents a compromise with respect to computational cost and accuracy between calculation of finite element approximations in higher-order finite element spaces and methods of pure interpolation. Instead of solving the globally coupled problem, local auxiliary problems are examined. This has sucessfully been applied to Poisson's problem in the framework of error estimators for global error norms [BW85, Ver96]. We propose in that context the solution of local Dirichlet problems embedded in defect correction steps associated to the considered higher-order finite element discretization. A solution of the dual problem is approximated in a conforming higher-order finite element space $\hat{V}_{1,h}^{(D)} \times \hat{V}_{2,h}^{(D)} \subset V_1^{(D)} \times V_2^{(D)}$. Due to the linear character of the dual problem and the divergence-free condition the linear system to be solved has the following saddle point structure:

$$\underbrace{\begin{bmatrix} A & B^T \\ B & 0 \end{bmatrix}}_{=:\mathcal{A}} \begin{bmatrix} z \\ q \end{bmatrix} = \begin{bmatrix} j^{(v)} \\ j^{(p)} \end{bmatrix}.$$

This problem is solved using a preconditioned Richardson iteration of the following form:

$$\begin{bmatrix} z_{i+1} \\ q_{i+1} \end{bmatrix} := \begin{bmatrix} z_i \\ q_i \end{bmatrix} + \omega C^{-1} \begin{bmatrix} Res_i^z \\ Res_i^q \end{bmatrix}, \tag{19}$$

with relaxation parameter ω. The block triangular preconditioning matrix C and the defect are defined by:

$$C := \begin{bmatrix} \tilde{A} & B^T \\ 0 & I \end{bmatrix}, \tag{20}$$

$$\begin{bmatrix} Res_i^z \\ Res_i^q \end{bmatrix} := \begin{bmatrix} j^{(v)} \\ j^{(p)} \end{bmatrix} - \begin{bmatrix} A & B^T \\ B & 0 \end{bmatrix} \begin{bmatrix} z_i \\ q_i \end{bmatrix}, \tag{21}$$

where the matrix I denotes the identity. $\tilde{A}$ has the same entries as A, except for each index n that corresponds to a degree of freedom (DOF) of the velocity on any cell's boundary (see accentuated DOFs in Figure 1):

$$\tilde{A}_{n,m} := \begin{cases} 0 & \text{, if } n \text{ corresponds to a DOF on cell boundary, } n \neq m \\ 1 & \text{, if } n \text{ corresponds to a DOF on cell boundary, } n = m \\ A_{n,m} & \text{, else.} \end{cases}$$

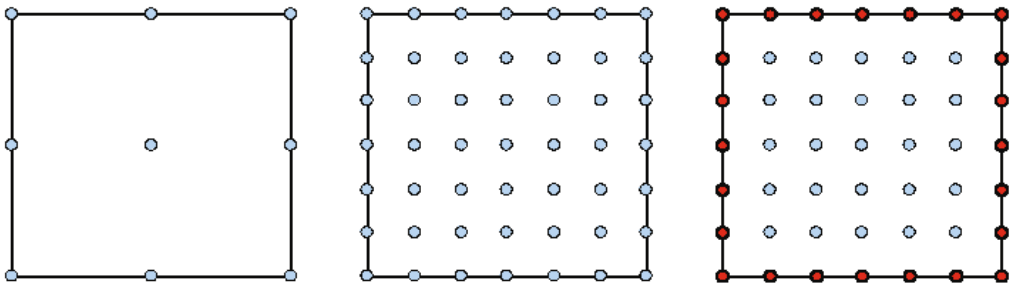

Fig. 1: Degrees of freedom on initial and higher-order FE space; highlighted DOFs on cell boundary

The discrete dual solution $(z_h, p_h) \in V_{1,h}^{(D)} \times V_{2,h}^{(D)}$ is supposed to be known. The starting point $(z_0, p_0) \in \hat{V}_{1,h}^{(D)} \times \hat{V}_{2,h}^{(D)}$ of the iteration (19) can be calculated by the *General Transfer Operator* [Sch00]

$$\hat{I}_h : V_{1,h}^{(D)} \times V_{2,h}^{(D)} \to \hat{V}_{1,h}^{(D)} \times \hat{V}_{2,h}^{(D)},$$

which is a change of basis in the case of subspaces $(V_{1,h}^{(D)} \times V_{2,h}^{(D)} \subset \hat{V}_{1,h}^{(D)} \times \hat{V}_{2,h}^{(D)})$. Hence the starting point is defined by

$$(z_0, p_0) := \hat{I}_h(z_h, q_h).$$

In Figure 1 a cell with the degrees of freedom of the initial finite element space (left) and the degrees of freedom of the higher-order finite element space (middle) are plotted. The iteration (19) converges, if the spectral radius of the iteration matrix $I - \omega C^{-1}\mathcal{A}$ is smaller than one.

In the preconditioning step, due to the definition of $\tilde{A}$, all degrees of freedom corresponding to the velocity variable on any cell's boundary are fixed. Hence the number of unknowns are smaller compared to the original problem. Further the couplings range over DOFs within single cells only. Hence the correction quantity $(Corr_i^z, Corr_i^q)^T$ can be calculated indepently and in parallel. The matrix $\tilde{A}$ can be reordered such that it consists of independent blocks, where each block corresponds to one cell. Each cell-wise problem has the form (cell $K \in \mathcal{T}_h$, iteration i)

$$\omega \begin{bmatrix} \tilde{A}_K & B_K^T \\ 0 & I_K \end{bmatrix}^{-1} \begin{bmatrix} Res_{K,i}^z \\ Res_{K,i}^q \end{bmatrix} = \begin{bmatrix} Cor_{K,i}^z \\ Cor_{K,i}^q \end{bmatrix}, \tag{22}$$

and represents a Dirichlet problem for cell K. Such local problems can be solved very efficiently in parallel. Only the computation of the residual is a global operation which takes into account the global couplings of the problem. But this is in general not very computational expensive in the overall solution procedure and its computation has good parallelization potential. The numerical tests described in Section 5 show, that even one or two numbers of iteration yield reliable a posteriori error estimates.

The application of this procedure is denoted by the operator $\mathcal{B} : V_{1,h}^{(D)} \times V_{2,h}^{(D)} \to \hat{V}_{1,h}^{(D)} \times \hat{V}_{2,h}^{(D)}$, i.e. the approximation of the exact solution is given by $(\hat{z}_h, \hat{q}_h) := \mathcal{B}(z_h, q_h)$. The primal residual that is evaluated for the error estimation has the following form

$$\rho((v_h, p_h); \mathcal{B}(z_h, q_h) - I_h(\mathcal{B}(z_h, q_h))).$$

Approximate solutions $(\hat{u}_h, \hat{p_h})$ of the primal problem can analogously be calculated by principle. In this case, the local matrices within the Richardson iteration (19) represent linearizations

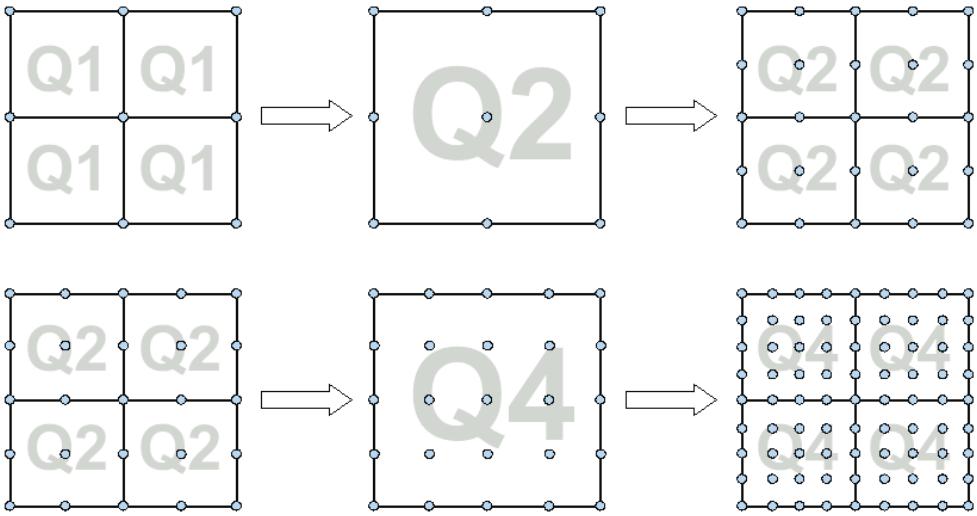

Fig. 2: Four small cells form one bigger cell with higher finite element ansatz

of the non-linear system and depend on the iteration step, i.e. $\tilde{A}_K \equiv \tilde{A}_K^i$. Still, the calculation of the correction term can be done independently for each cell in parallel. A big advantage of this iterative procedure lies in the possibility to control the computational costs and accuracy by determining the number of iterations.

4.3 Higher-order interpolation

The main drawback of the methods described previously is related to the comparatively high computational costs associated to the higher-order elements, even if only needed locally as proposed in Section 4.2. In practice, a commonly used approach relies on extrapolation techniques taking advantage of patch structure of the considered mesh. Theoretically, theses techniques are only valid under strong regularity assumption both with respect to the mesh and the solution. However these methods are used in a much wider setup, since they rely on the definition of an adequate interpolation operator, which is usually computationally quite cheap. To the knowledge of the authors the impact of the associated error on the quality of the error estimation is at least theoretically still an open question.

The considered interpolation scheme can be applied very efficiently to meshes that consist of patches. This means that the mesh can be coarsened such that four neighboring cells form one cell in the coarsened mesh (see Figure 2). For ease of presentation we assume Taylor-Hood elements [BF91] for the discretization. The idea of higher-order interpolation as described in [BR03] is to interpret the finite elements in a patch consisting of four cells (in 2D) as one finite element in the common father cell. Therefore the degrees of freedom of the four cells with finite element ansatz Qn, $n \in \{1, 2\}$, are used as degrees of freedom in the father cell which has finite element ansatz Qm, where $m = 2n$. By Qm-interpolation on the patch cell it is easy to calculate the values for the degrees of freedom that correspond to an Qm ansatz on each of the four initial cells such that the higher-order interpolation is given by an Qm ansatz on each cell, what might be technically convenient as the interpolated solution can be represented on the same cells as the initial finite element solution.In Figure 2 for the case of $Q1$ and $Q2$ cells, a patch of four cells (left) and the corresponding patch cell (middle) is shown. The patch of higher-order cells (right) show the cells with higher-order finite elements which is just an other representation

of the same interpolated solution (change of basis). Degrees of freedom that correspond to the particular finite element ansatz are indicated by points. In meshes that don't have patch structure, for each cell a virtual patch cell can be defined and used for the interpolation, which is computationally more expensive. We refer e.g. to [CH08] for more details.

As $I_h(\hat{I}_{2h}(u_h)) = u_h$ and $I_h(\hat{I}_{2h}(z_h)) = z_h$ in this special situation, no extra interpolation needs to be calculated. The residuals that are evaluated for the error characterizations have the form

$$\rho(u_h; \hat{I}_{2h}(z_h) - z_h), \quad \rho^*_{u_h}(z_h; \hat{I}_{2h}(u_h) - u_h).$$

5 Numerical simulation

In the following the presented goal oriented adaptive techniques are applied to scenarios with known analytical solution in order to quantify the reliability and efficiency of the error estimators based on the different strategies to approximate the exact primal and dual solution, presented in Section 4. All scenarios have been chosen to be related to configurations and setups which are associated to problems occuring in meteorology and climate research. For each scenario and each goal functional, the reference solution was evaluated using the computer algebra system Maple$^{\text{TM}}$ [MGH+05]. For the discretization with finite elements the domain $\Omega \subset \mathbb{R}^2$ is partitioned into quadrilaterals. Taylor-Hood elements are used, which are globally continuous and piecewise bi-quadratic for the velocity components and piecewise bi-linear for the pressure component in the simplest case. The global form functions have for degree i the following form:

$$V_{1,h} := \left\{ v_h \in H^1_0(\Omega)^2 : v_{h|K} \in Q^2_i(K)\ \forall K \in \mathcal{T}_h,\ v_h = 0 \text{ on } \Gamma \right\},$$
$$V_{2,h} := \left\{ p_h \in L^2(\Omega) : p_{h|K} \in Q_{i-1}(K)\ \forall K \in \mathcal{T}_h, \int_\Omega p_h\, dx = 0 \right\}.$$

Here $Q_i(K)$ denotes the polynomials with maximal degree of i in each variable defined on cell K, that is in two space dimensions

$$Q_i(K) := \left\{ u(x,y) = \sum_{0 \le s,t \le i} c_{st} x^s y^t,\ (x,y) \in K \right\}.$$

It can be shown that for $i \ge 2$ these elements fulfill the LBB-condition [Bre74] and therefore are stable [BF91]. Taylor-Hood elements with polynomial degree 2 for the velocity are called Q2Q1 elements and are the default finite element space of the primal and dual problem in the following numerical simulations. In the following QnQm denotes Taylor-Hood elements, where n and m denote the polynomial degree of the velocity components and pressure field, respectively. In h-adapted meshes consisting of quadrilateral cells only, so-called *hanging nodes* exist that have to be treated in a way such that global conformity is guaranteed, which is a global continuity condition in the case of H^1-conforming spaces. We consider the approach presented in [HS07, HR03].

In the following, the adaptive method is described. For each adaptation cycle, first the discrete primal and dual solutions are calculated. Then based on different strategies the error quantities (17) can be evaluated and for each cell the local error contribution can be estimated in terms of the local indicators η_K and η^*_K. Many mesh adaptation strategies aim to iterate towards an equally distributed error contribution of each cell $K \in \mathcal{T}_h$. Hence, cells are marked for refinement or coarsening that have too large or too small error indication with respect to some criterion. We used for all adaptive numerical simulations the same mesh refinement strategy. For a parameter $0 \le \alpha \le 1$ and the maximal error indicator $\eta_{max} := \max_{K \in \mathcal{T}_h}\{\eta_K\}$ in the current mesh, the set

$$A := \{K \in \mathcal{T}_h : \eta_K \ge \alpha \eta_{max}\}$$

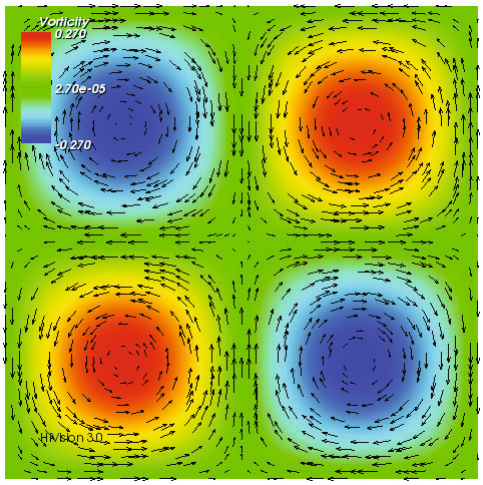

Fig. 3: Taylor-Green vortex: Velocity field, colored by vorticity

contains the cells that should be refined. For symmetrical scenarios, this strategy allows the same treatment of cells with identical error indication leading to symmetrical meshes. The parameter α is chosen as $1/16$.

All numerical simulations were performed using the multi-purpose finite element library HiFlow^3 [AAB+10]. The visualizations of the solutions and weight functions were generated using the visualization platform HiVision [BH06]. The evaluation of the reference values of the goals for the scenarios were calculated using Maple$^{\text{TM}}$ [MGH+05].

5.1 Taylor-Green vortex

The first configuration is the well-known Taylor-Green vortex [Cho68]. The velocity and pressure distribution that fulfills the Navier-Stokes equations is given by

$$\begin{aligned} v_1(x,y) &:= -e^{-2}\cos(x)\sin(y), \\ v_2(x,y) &:= e^{-2}\sin(x)\cos(y), \\ p(x,y) &:= -e^{-4}(\cos(2x)+\cos(2y))/4, \end{aligned}$$

defined in the domain $\Omega = [\frac{1}{2}\pi;\frac{5}{2}\pi]^2$. Figure 3 shows the velocity field consisting of four vortices. The glyphs represent the velocity field and the coloring is based on the vorticity, where blue regions mark clock-wise and red regions mark counter-clock-wise vortical structures. The corresponding right-hand side of the Navier-Stokes equations with kinematic viscosity $\nu = 1$ and density $\rho = 1$ is

$$\begin{aligned} f_1(x,y) &= -2e^{-2}\cos(x)\sin(y), \\ f_2(x,y) &= 2e^{-2}\sin(x)\cos(y). \end{aligned}$$

5.1.1 Scenario 1: Point value of velocity

Given a point $\hat{x} \in \Omega$, the quantity of interest is defined as the x-component of the velocity at this point:

$$J_1(v,p) := v_1(\hat{x}) \approx \frac{1}{|B(\hat{x},\epsilon)|}\int_{B(\hat{x},\epsilon)} v_1(x)\,dx.$$

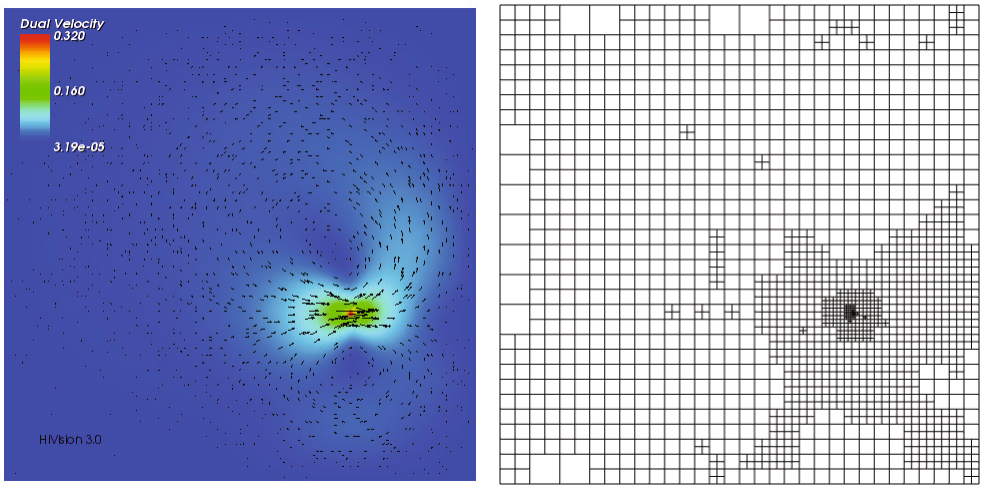

Fig. 4: Point value of velocity, scenario 1: (left) dual velocity and (right) optimized mesh

Here $B(\hat{x}, \epsilon)$ is a ball with radius $\epsilon > 0$, centered at $\hat{x}$ and $|B(\hat{x}, \epsilon)|$ is its surface. The radius is defined as $\epsilon := \epsilon(h_{min}) := h_{min}/4$, where $h_{min} := \min_{K \in \mathcal{T}_h} \{\operatorname{diam} K\}$ is the smallest cell diameter in the mesh. For point $\hat{x} = (6.2, 3.8)$ the reference value is

$$J_1(v, p) \approx 0.082519625992351.$$

5.1.2 Scenario 2: Weighted integral of vorticity (I)

For the weight function

$$w_1(x) := \sin\left(-\frac{x_1^2}{4\pi} + \frac{5x_1}{4} - \frac{9\pi}{16}\right) \sin\left(-\frac{x_2^2}{4\pi} + \frac{5x_2}{4} - \frac{9\pi}{16}\right), \quad x \in \Omega$$

the weighted integral of the vorticity

$$J_2(v, p) := \int_\Omega w_1(x) \cdot \nabla \times v(x)\, dx \approx 0.422120125202319$$

is chosen as goal functional.

5.1.3 Scenario 3: Weighted integral of vorticity (II)

For point $\tilde{x} = (3.0, 4.0)$, the weight function with small support close to $\tilde{x}$ is defined by

$$w_2(x) := \begin{cases} \exp\left(\frac{1}{(x_1 - \tilde{x}_1)^2 - 1} + \frac{1}{(x_2 - \tilde{x}_2)^2 - 1}\right), & \text{if } \|x - \tilde{x}\|_\infty \leq 1 \\ 0, & \text{else} \end{cases}.$$

The goal functional is defined as the weighted integral of vorticity

$$J_3(v, p) := \int_\Omega w_2(x) \cdot \nabla \times v(x)\, dx \approx 0.029422745464403.$$

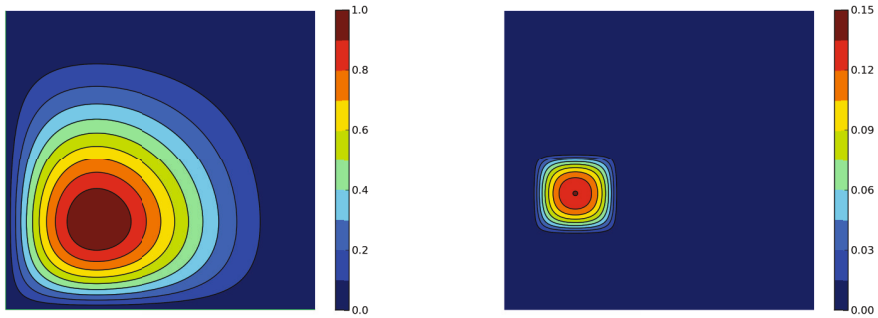

Fig. 5: Weight function ω_1 related to scenario 2 (left), weight function ω_2 related to scenario 3 (right)

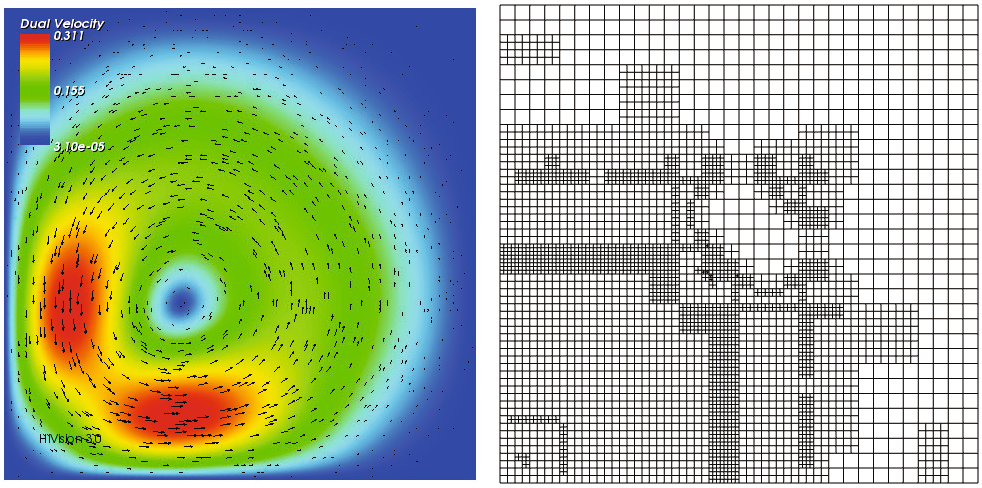

Fig. 6: Weighted integral of vorticity (I), scenario 2: (left) dual velocity and (right) optimized mesh

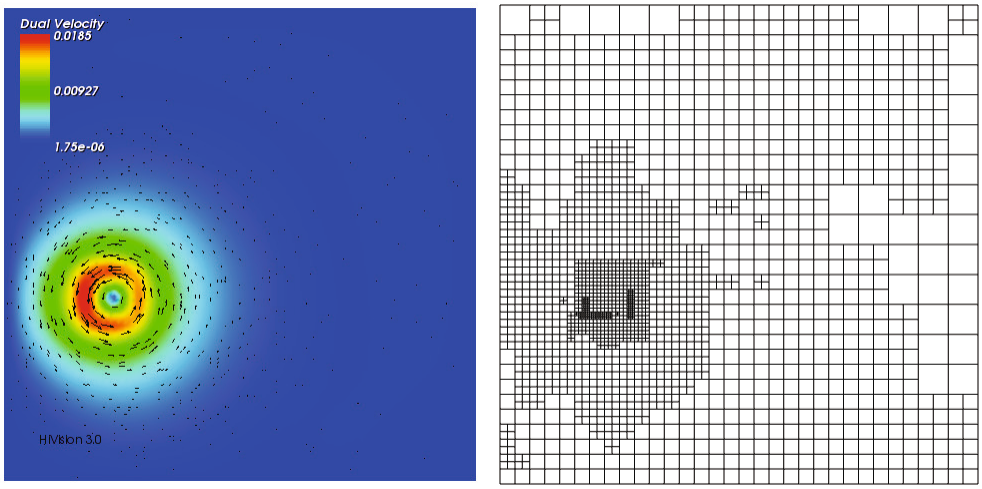

Fig. 7: Weighted integral of vorticity (II), scenario 3: (left) dual velocity and (right) optimized mesh

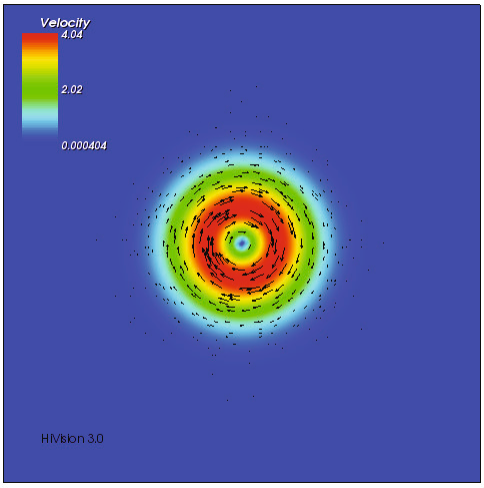

Fig. 8: Single vortex: Velocity field, colored by norm of velocity

5.2 Single vortex

The second configuration contains a monopolar vortex with smooth vorticity profile and azimuthal velocity, called *Gaussian vort*ex, as used e.g. by Scheck et al. [SJJ11] to describe idealised tropical cyclones. The exact solution is defined by the following velocity and pressure distribution in the domain $\Omega := [-1,1]^2$:

$$\begin{aligned} v_1(x,y) &:= \frac{y}{r_0^2} \cdot e^{-\frac{x^2+y^2}{2r_0^2}}, \\ v_2(x,y) &:= -\frac{x}{r_0^2} \cdot e^{-\frac{x^2+y^2}{2r_0^2}}, \\ p(x,y) &:= -\frac{\rho}{2r_0^2} \cdot e^{-\frac{x^2+y^2}{r_0^2}}. \end{aligned}$$

The radius parameters is $r_0 = 0.15$, the kinematic viscosity is $\nu = 1$ and the density is $\rho = 1$. The corresponding right-hand side of the Navier-Stokes equations is defined as

$$\begin{aligned} f_1(x,y) &= \frac{\nu y(4r_0^2 - x^2 - y^2)}{r_0^6} \cdot e^{-\frac{x^2+y^2}{2r_0^2}}, \\ f_2(x,y) &= -\frac{\nu x(4r_0^2 - x^2 - y^2)}{r_0^6} \cdot e^{-\frac{x^2+y^2}{2r_0^2}} \end{aligned}$$

and corresponds to effects of viscosity as (v_1, v_2, p) is a solution of the Euler equations with homogeneous right-hand side.

5.2.1 Scenario 4: Point value of vorticity

For point $x_0 = (0.35, 0.45)$ the vorticity at that point

$$J_4(v,p) := \nabla \times v(x_0) \approx \frac{1}{|B(x_0,\epsilon)|} \int_{B(x_0,\epsilon)} \nabla \times v(x)\, dx$$

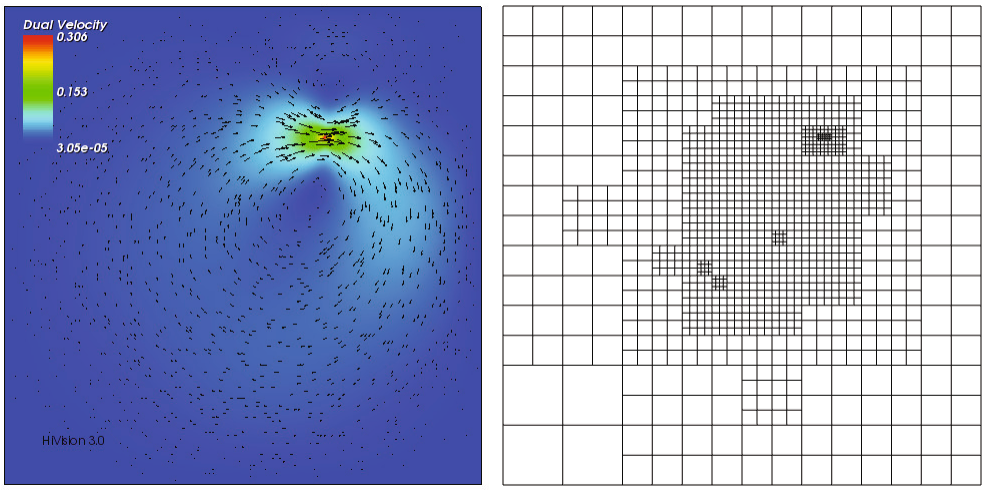

Fig. 9: Point value of vorticity, scenario 3: (left) dual velocity and (right) optimized mesh

is of interest in this investigaation. Again $B(x_0, \epsilon)$ is a ball with radius $\epsilon > 0$, centered at x_0 and $|B(x_0, \epsilon)|$ its surface and $\epsilon := \epsilon(h_{min}) := h_{min}/4$, where $h_{min} := \min_{K \in \mathcal{T}_h} \{\operatorname{diam} K\}$ is the smallest cell diameter in the current mesh. The vorticity at point x_0 can be evaluated to be

$$J_4(v, p) \approx 0.403851534372451.$$

5.2.2 Scenario 5: Kinetic energy

The goal functional is defined as the kinetic energy in the domain Ω:

$$J_5(v, p) := \|v\|_\Omega^2 = (v, v)_\Omega = \int_\Omega v(x) \cdot v(x)\, dx.$$

Because this functional is non-linear, the right-hand side of the dual problem is its linearization, see Equation (13):

$$\begin{aligned}
\nabla_v J_5(v, p)(\varphi) &= \lim_{\lambda \to 0} \frac{J_5(v + \lambda\varphi, p) - J_5(v, p)}{\lambda} \\
&= \lim_{\lambda \to 0} \frac{1}{\lambda} \left[(v + \lambda\varphi, v + \lambda\varphi)_\Omega - (v, v)_\Omega\right] \\
&= \lim_{\lambda \to 0} \frac{1}{\lambda} \left[(v, v)_\Omega + 2\lambda(v, \varphi)_\Omega + \lambda^2(\varphi, \varphi)_\Omega - (v, v)_\Omega\right] \\
&= 2(v, \varphi)_\Omega.
\end{aligned}$$

The integrated kinetic energy approximately is

$$J_5(v, p) \approx 3.141592653589793.$$

5.3 Description of the adaptive numerical simulations

In order to better quantify the quality of the different variants of the error estimators, we consider for each scenario and estimator variant sequences of globally, i.e. regular, and adaptively refined

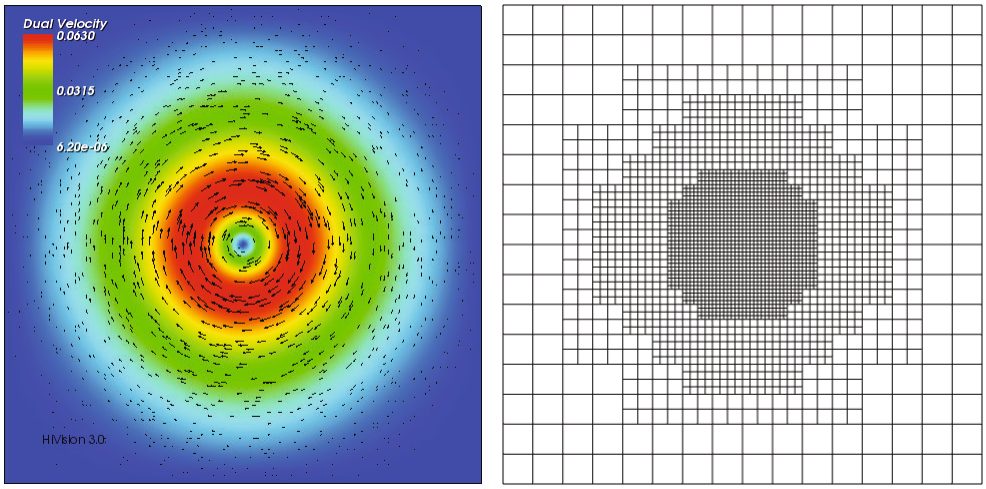

Fig. 10: Kinetic Energy, scenario 5: (left) dual velocity and (right) optimized mesh

meshes. On globally refined meshes the number of degrees of freedom is common for all variants which allows a comparison of the efficiency of the error estimators in a common context. For this investigation the *efficiency index* is introduced:

$$I_{\text{eff}} := \left| \frac{E(u_h)}{J(u) - J(u_h)} \right|, \tag{23}$$

and should optimally be close to one, i.e. the estimated error is close to the true error. Here $E(u_h)$ denotes the estimated error for the variants E_P, E_D and E_{PD} as defined by (6). For all simulations, the finite element solutions are Q2Q1 functions. The finite element spaces for the approximations of the exact primal and dual problem are:

Strategy	Elements
Higher-order finite element approximation	Q3Q2
Block strategy	Q3Q2
Higher-order interpolation	Q4Q2

In the following the results of the numerical simulations are described in a sequence of tabulars and plots. The tabulars describe the efficiency index, the estimated error $E(u_h)$, the true error in J – defined as difference between reference value and the approximate value $J(u_h)$ – and the error of the improved value $\tilde{J}(u_h)$, see Equation (7). The plots include the efficiency indicator I_{eff} and true error in J of the adaptive and corresponding globally refined runs to investigate the relation between accuracy and number of unknowns.

5.3.1 Point-value of velocity

# DOFs	$\lvert J(u) - J(u_h)\rvert$	$\lvert E(u_h)\rvert$	I_{eff}	$\lvert J(u) - \tilde{J}(u_h)\rvert$
659	$4.84 \cdot 10^{-04}$	$2.78 \cdot 10^{-04}$	0.57	$2.06 \cdot 10^{-04}$
2467	$4.85 \cdot 10^{-05}$	$2.77 \cdot 10^{-05}$	0.57	$2.07 \cdot 10^{-05}$
9539	$4.28 \cdot 10^{-06}$	$2.51 \cdot 10^{-06}$	0.59	$1.76 \cdot 10^{-06}$
37507	$6.95 \cdot 10^{-07}$	$3.70 \cdot 10^{-07}$	0.53	$3.24 \cdot 10^{-07}$
148739	$4.94 \cdot 10^{-08}$	$2.91 \cdot 10^{-08}$	0.59	$2.03 \cdot 10^{-08}$

Tab. 1: Scenario 1, D, analytical solution of primal problem, interpolation

# DOFs	$\lvert J(u) - J(u_h)\rvert$	$\lvert E(u_h)\rvert$	I_{eff}	$\lvert J(u) - \tilde{J}(u_h)\rvert$
659	$4.84 \cdot 10^{-04}$	$2.71 \cdot 10^{-04}$	0.56	$2.13 \cdot 10^{-04}$
2467	$4.85 \cdot 10^{-05}$	$2.67 \cdot 10^{-05}$	0.55	$2.18 \cdot 10^{-05}$
9539	$4.28 \cdot 10^{-06}$	$2.61 \cdot 10^{-06}$	0.61	$1.66 \cdot 10^{-06}$
37507	$6.95 \cdot 10^{-07}$	$3.67 \cdot 10^{-07}$	0.53	$3.27 \cdot 10^{-07}$
148739	$4.94 \cdot 10^{-08}$	$2.95 \cdot 10^{-08}$	0.60	$1.99 \cdot 10^{-08}$

Tab. 2: Scenario 1, P, higher-order finite element solution

# DOFs	$\lvert J(u) - J(u_h)\rvert$	$\lvert E(u_h)\rvert$	I_{eff}	$\lvert J(u) - \tilde{J}(u_h)\rvert$
659	$4.84 \cdot 10^{-04}$	$2.81 \cdot 10^{-04}$	0.58	$2.03 \cdot 10^{-04}$
2467	$4.85 \cdot 10^{-05}$	$2.73 \cdot 10^{-05}$	0.56	$2.12 \cdot 10^{-05}$
9539	$4.28 \cdot 10^{-06}$	$2.57 \cdot 10^{-06}$	0.60	$1.70 \cdot 10^{-06}$
37507	$6.95 \cdot 10^{-07}$	$3.70 \cdot 10^{-07}$	0.53	$3.25 \cdot 10^{-07}$
148739	$4.94 \cdot 10^{-08}$	$2.93 \cdot 10^{-08}$	0.59	$2.01 \cdot 10^{-08}$

Tab. 3: Scenario 1, PD, higher-order finite element solution

# DOFs	$\lvert J(u) - J(u_h)\rvert$	$\lvert E(u_h)\rvert$	I_{eff}	$\lvert J(u) - \tilde{J}(u_h)\rvert$
659	$4.84 \cdot 10^{-04}$	$4.61 \cdot 10^{-05}$	0.10	$4.38 \cdot 10^{-04}$
2467	$4.85 \cdot 10^{-05}$	$1.86 \cdot 10^{-05}$	0.38	$2.99 \cdot 10^{-05}$
9539	$4.28 \cdot 10^{-06}$	$2.87 \cdot 10^{-06}$	0.67	$7.15 \cdot 10^{-06}$
37507	$6.95 \cdot 10^{-07}$	$2.30 \cdot 10^{-07}$	0.33	$9.25 \cdot 10^{-07}$
148739	$4.94 \cdot 10^{-08}$	$4.26 \cdot 10^{-08}$	0.86	$9.20 \cdot 10^{-08}$

Tab. 4: Scenario 1, P, higher-order interpolation

# DOFs	$\lvert J(u) - J(u_h)\rvert$	$\lvert E(u_h)\rvert$	I_{eff}	$\lvert J(u) - \tilde{J}(u_h)\rvert$
659	$4.84 \cdot 10^{-04}$	$1.82 \cdot 10^{-04}$	0.38	$3.02 \cdot 10^{-04}$
2467	$4.85 \cdot 10^{-05}$	$2.45 \cdot 10^{-05}$	0.51	$2.40 \cdot 10^{-05}$
9539	$4.28 \cdot 10^{-06}$	$2.25 \cdot 10^{-07}$	0.05	$4.50 \cdot 10^{-06}$
37507	$6.95 \cdot 10^{-07}$	$6.77 \cdot 10^{-08}$	0.10	$6.27 \cdot 10^{-07}$
148739	$4.94 \cdot 10^{-08}$	$6.88 \cdot 10^{-09}$	0.14	$5.63 \cdot 10^{-08}$

Tab. 5: Scenario 1, PD, higher-order interpolation

# DOFs	$\lvert J(u) - J(u_h)\rvert$	$\lvert E(u_h)\rvert$	I_{eff}	$\lvert J(u) - \tilde{J}(u_h)\rvert$
659	$4.84 \cdot 10^{-04}$	$1.43 \cdot 10^{-04}$	0.29	$3.42 \cdot 10^{-04}$
2467	$4.85 \cdot 10^{-05}$	$1.47 \cdot 10^{-05}$	0.30	$3.38 \cdot 10^{-05}$
9539	$4.28 \cdot 10^{-06}$	$5.92 \cdot 10^{-07}$	0.14	$3.68 \cdot 10^{-06}$
37507	$6.95 \cdot 10^{-07}$	$1.79 \cdot 10^{-07}$	0.26	$5.16 \cdot 10^{-07}$
148739	$4.94 \cdot 10^{-08}$	$1.33 \cdot 10^{-08}$	0.27	$3.61 \cdot 10^{-08}$

Tab. 6: Scenario 1, P, block strategy, one update step, $\omega = 0.2$

# DOFs	$\lvert J(u) - J(u_h)\rvert$	$\lvert E(u_h)\rvert$	I_{eff}	$\lvert J(u) - \tilde{J}(u_h)\rvert$
659	$4.84 \cdot 10^{-04}$	$1.61 \cdot 10^{-04}$	0.33	$3.23 \cdot 10^{-04}$
2467	$4.85 \cdot 10^{-05}$	$1.65 \cdot 10^{-05}$	0.34	$3.20 \cdot 10^{-05}$
9539	$4.28 \cdot 10^{-06}$	$9.11 \cdot 10^{-07}$	0.21	$3.37 \cdot 10^{-06}$
37507	$6.95 \cdot 10^{-07}$	$1.82 \cdot 10^{-07}$	0.26	$5.13 \cdot 10^{-07}$
148739	$4.94 \cdot 10^{-08}$	$1.71 \cdot 10^{-08}$	0.35	$3.23 \cdot 10^{-08}$

Tab. 7: Scenario 1, P, block strategy, two update steps, $\omega = 0.2$

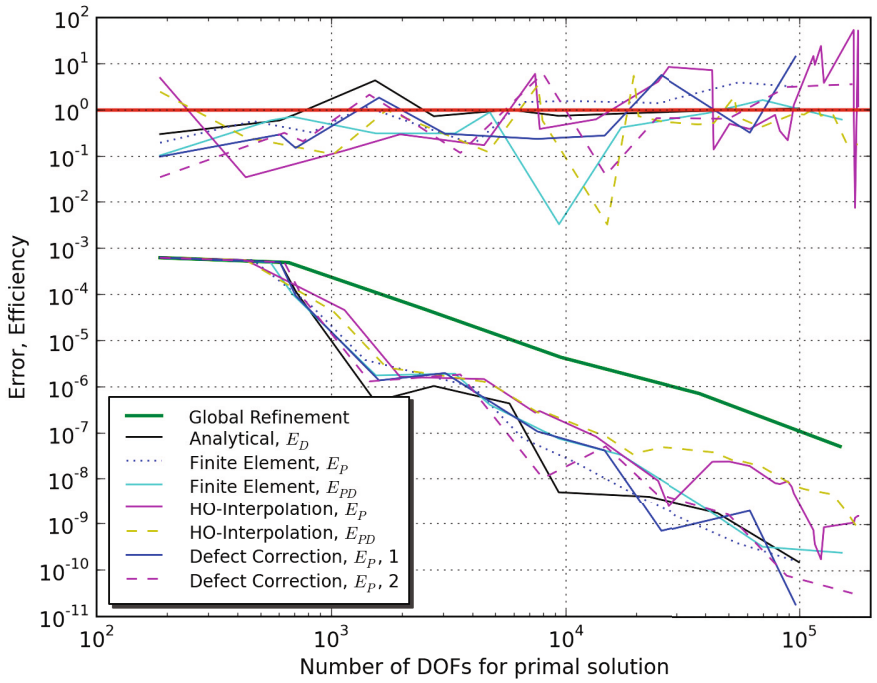

Fig. 11: Error and efficiency plots for scenario 1

5.3.2 Weighted integral of vorticity (I)

# DOFs	$\lvert J(u) - J(u_h)\rvert$	$\lvert E(u_h)\rvert$	I_{eff}	$\lvert J(u) - \tilde{J}(u_h)\rvert$
659	$3.16 \cdot 10^{-04}$	$3.16 \cdot 10^{-04}$	1.00	$5.68 \cdot 10^{-08}$
2467	$1.95 \cdot 10^{-05}$	$1.95 \cdot 10^{-05}$	1.00	$7.67 \cdot 10^{-10}$
9539	$1.22 \cdot 10^{-06}$	$1.22 \cdot 10^{-06}$	1.00	$1.38 \cdot 10^{-11}$
37507	$7.61 \cdot 10^{-08}$	$7.61 \cdot 10^{-08}$	1.00	$2.39 \cdot 10^{-12}$
148739	$4.75 \cdot 10^{-09}$	$4.76 \cdot 10^{-09}$	1.00	$2.10 \cdot 10^{-12}$

Tab. 8: Scenario 2, D, analytical solution of primal problem, interpolation

# DOFs	$\lvert J(u) - J(u_h)\rvert$	$\lvert E(u_h)\rvert$	I_{eff}	$\lvert J(u) - \tilde{J}(u_h)\rvert$
659	$3.16 \cdot 10^{-04}$	$2.24 \cdot 10^{-04}$	0.71	$9.25 \cdot 10^{-05}$
2467	$1.95 \cdot 10^{-05}$	$1.40 \cdot 10^{-05}$	0.72	$5.53 \cdot 10^{-06}$
9539	$1.22 \cdot 10^{-06}$	$8.74 \cdot 10^{-07}$	0.72	$3.44 \cdot 10^{-07}$
37507	$7.61 \cdot 10^{-08}$	$5.45 \cdot 10^{-08}$	0.72	$2.16 \cdot 10^{-08}$
148739	$4.75 \cdot 10^{-09}$	$3.40 \cdot 10^{-09}$	0.72	$1.35 \cdot 10^{-09}$

Tab. 9: Scenario 2, P, higher-order finite element solution

# DOFs	$\lvert J(u) - J(u_h)\rvert$	$\lvert E(u_h)\rvert$	I_{eff}	$\lvert J(u) - \tilde{J}(u_h)\rvert$
659	$3.16 \cdot 10^{-04}$	$2.85 \cdot 10^{-04}$	0.90	$3.18 \cdot 10^{-05}$
2467	$1.95 \cdot 10^{-05}$	$1.77 \cdot 10^{-05}$	0.91	$1.85 \cdot 10^{-06}$
9539	$1.22 \cdot 10^{-06}$	$1.10 \cdot 10^{-06}$	0.91	$1.15 \cdot 10^{-07}$
37507	$7.61 \cdot 10^{-08}$	$6.89 \cdot 10^{-08}$	0.91	$7.18 \cdot 10^{-09}$
148739	$4.75 \cdot 10^{-09}$	$4.31 \cdot 10^{-09}$	0.91	$4.48 \cdot 10^{-10}$

Tab. 10: Scenario 2, PD, higher-order finite element solution

# DOFs	$\lvert J(u) - J(u_h)\rvert$	$\lvert E(u_h)\rvert$	I_{eff}	$\lvert J(u) - \tilde{J}(u_h)\rvert$
659	$3.16 \cdot 10^{-04}$	$1.89 \cdot 10^{-04}$	0.60	$1.27 \cdot 10^{-04}$
2467	$1.95 \cdot 10^{-05}$	$1.34 \cdot 10^{-05}$	0.68	$6.16 \cdot 10^{-06}$
9539	$1.22 \cdot 10^{-06}$	$8.66 \cdot 10^{-07}$	0.71	$3.52 \cdot 10^{-07}$
37507	$7.61 \cdot 10^{-08}$	$5.45 \cdot 10^{-08}$	0.72	$2.16 \cdot 10^{-08}$
148739	$4.75 \cdot 10^{-09}$	$3.41 \cdot 10^{-09}$	0.72	$1.35 \cdot 10^{-09}$

Tab. 11: Scenario 2, P, higher-order interpolation

# DOFs	$\lvert J(u) - J(u_h)\rvert$	$\lvert E(u_h)\rvert$	I_{eff}	$\lvert J(u) - \tilde{J}(u_h)\rvert$
659	$3.16 \cdot 10^{-04}$	$2.61 \cdot 10^{-04}$	0.82	$5.57 \cdot 10^{-05}$
2467	$1.95 \cdot 10^{-05}$	$1.66 \cdot 10^{-05}$	0.85	$2.93 \cdot 10^{-06}$
9539	$1.22 \cdot 10^{-06}$	$1.04 \cdot 10^{-06}$	0.86	$1.74 \cdot 10^{-07}$
37507	$7.61 \cdot 10^{-08}$	$6.53 \cdot 10^{-08}$	0.86	$1.08 \cdot 10^{-08}$
148739	$4.75 \cdot 10^{-09}$	$4.08 \cdot 10^{-09}$	0.86	$6.72 \cdot 10^{-10}$

Tab. 12: Scenario 2, PD, higher-order interpolation

# DOFs	$\lvert J(u) - J(u_h)\rvert$	$\lvert E(u_h)\rvert$	I_{eff}	$\lvert J(u) - \tilde{J}(u_h)\rvert$
659	$3.16 \cdot 10^{-04}$	$9.86 \cdot 10^{-05}$	0.31	$2.18 \cdot 10^{-04}$
2467	$1.95 \cdot 10^{-05}$	$6.19 \cdot 10^{-06}$	0.32	$1.34 \cdot 10^{-05}$
9539	$1.22 \cdot 10^{-06}$	$3.82 \cdot 10^{-07}$	0.31	$8.37 \cdot 10^{-07}$
37507	$7.61 \cdot 10^{-08}$	$2.36 \cdot 10^{-08}$	0.31	$5.25 \cdot 10^{-08}$
148739	$4.75 \cdot 10^{-09}$	$1.47 \cdot 10^{-09}$	0.31	$3.29 \cdot 10^{-09}$

Tab. 13: Scenario 2, P, block strategy, one update step, $\omega = 0.2$

# DOFs	$\lvert J(u) - J(u_h)\rvert$	$\lvert E(u_h)\rvert$	I_{eff}	$\lvert J(u) - \tilde{J}(u_h)\rvert$
659	$3.16 \cdot 10^{-04}$	$1.16 \cdot 10^{-04}$	0.37	$2.00 \cdot 10^{-04}$
2467	$1.95 \cdot 10^{-05}$	$7.14 \cdot 10^{-06}$	0.37	$1.24 \cdot 10^{-05}$
9539	$1.22 \cdot 10^{-06}$	$4.40 \cdot 10^{-07}$	0.36	$7.78 \cdot 10^{-07}$
37507	$7.61 \cdot 10^{-08}$	$2.73 \cdot 10^{-08}$	0.36	$4.88 \cdot 10^{-08}$
148739	$4.75 \cdot 10^{-09}$	$1.70 \cdot 10^{-09}$	0.36	$3.06 \cdot 10^{-09}$

Tab. 14: Scenario 2, P, block strategy, two update steps, $\omega = 0.2$

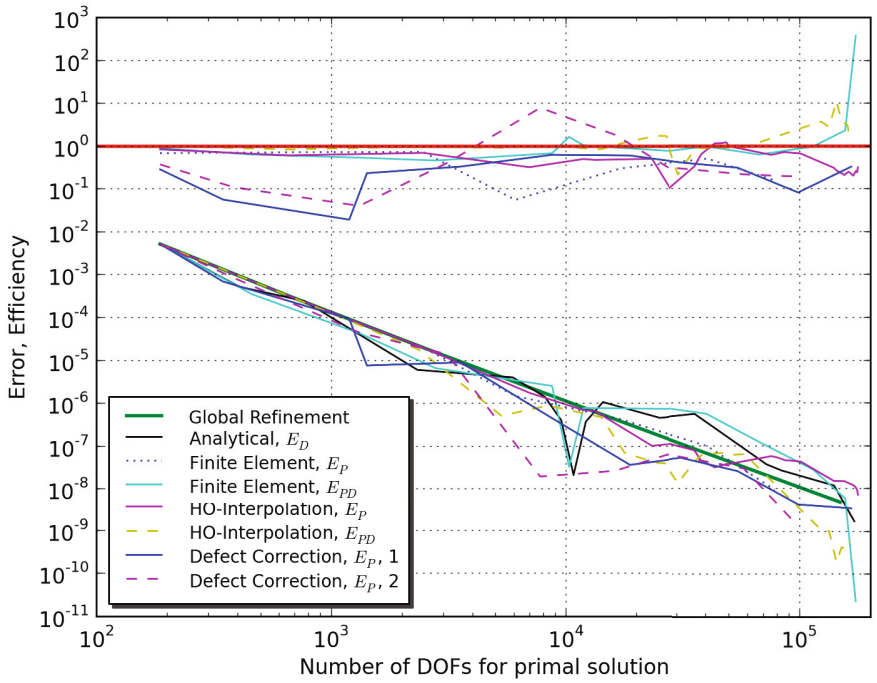

Fig. 12: Error and efficiency plots for scenario 2

5.3.3 Weighted integral of vorticity (II)

# DOFs	$\lvert J(u) - J(u_h)\rvert$	$\lvert E(u_h)\rvert$	I_{eff}	$\lvert J(u) - \tilde{J}(u_h)\rvert$
659	$2.44 \cdot 10^{-05}$	$2.95 \cdot 10^{-05}$	1.21	$5.03 \cdot 10^{-06}$
2467	$2.39 \cdot 10^{-06}$	$8.56 \cdot 10^{-07}$	0.36	$3.24 \cdot 10^{-06}$
9539	$1.33 \cdot 10^{-07}$	$3.62 \cdot 10^{-08}$	0.27	$9.70 \cdot 10^{-08}$
37507	$3.07 \cdot 10^{-09}$	$3.92 \cdot 10^{-09}$	1.28	$8.47 \cdot 10^{-10}$
148739	$9.07 \cdot 10^{-11}$	$7.96 \cdot 10^{-11}$	0.88	$1.11 \cdot 10^{-11}$

Tab. 15: Scenario 3, D, analytical solution of primal problem, interpolation

# DOFs	$\lvert J(u) - J(u_h)\rvert$	$\lvert E(u_h)\rvert$	I_{eff}	$\lvert J(u) - \tilde{J}(u_h)\rvert$
659	$2.44 \cdot 10^{-05}$	$3.14 \cdot 10^{-05}$	1.29	$7.01 \cdot 10^{-06}$
2467	$2.39 \cdot 10^{-06}$	$8.29 \cdot 10^{-07}$	0.35	$3.22 \cdot 10^{-06}$
9539	$1.33 \cdot 10^{-07}$	$3.23 \cdot 10^{-08}$	0.24	$1.01 \cdot 10^{-07}$
37507	$3.07 \cdot 10^{-09}$	$3.70 \cdot 10^{-09}$	1.21	$6.36 \cdot 10^{-10}$
148739	$9.07 \cdot 10^{-11}$	$6.54 \cdot 10^{-11}$	0.72	$2.53 \cdot 10^{-11}$

Tab. 16: Scenario 3, P, higher-order finite element solution

# DOFs	$\lvert J(u) - J(u_h)\rvert$	$\lvert E(u_h)\rvert$	I_{eff}	$\lvert J(u) - \tilde{J}(u_h)\rvert$
659	$2.44 \cdot 10^{-05}$	$3.09 \cdot 10^{-05}$	1.26	$6.43 \cdot 10^{-06}$
2467	$2.39 \cdot 10^{-06}$	$8.67 \cdot 10^{-07}$	0.36	$3.26 \cdot 10^{-06}$
9539	$1.33 \cdot 10^{-07}$	$3.47 \cdot 10^{-08}$	0.26	$9.86 \cdot 10^{-08}$
37507	$3.07 \cdot 10^{-09}$	$3.86 \cdot 10^{-09}$	1.26	$7.87 \cdot 10^{-10}$
148739	$9.07 \cdot 10^{-11}$	$7.48 \cdot 10^{-11}$	0.83	$1.58 \cdot 10^{-11}$

Tab. 17: Scenario 3, PD, higher-order finite element solution

# DOFs	$\lvert J(u) - J(u_h)\rvert$	$\lvert E(u_h)\rvert$	I_{eff}	$\lvert J(u) - \tilde{J}(u_h)\rvert$
659	$2.44 \cdot 10^{-05}$	$7.52 \cdot 10^{-06}$	0.31	$1.69 \cdot 10^{-05}$
2467	$2.39 \cdot 10^{-06}$	$1.19 \cdot 10^{-06}$	0.50	$1.19 \cdot 10^{-06}$
9539	$1.33 \cdot 10^{-07}$	$2.95 \cdot 10^{-08}$	0.22	$1.04 \cdot 10^{-07}$
37507	$3.07 \cdot 10^{-09}$	$2.23 \cdot 10^{-09}$	0.72	$8.44 \cdot 10^{-10}$
148739	$9.07 \cdot 10^{-11}$	$2.32 \cdot 10^{-10}$	2.56	$1.41 \cdot 10^{-10}$

Tab. 18: Scenario 3, P, higher-order interpolation

# DOFs	$\lvert J(u) - J(u_h)\rvert$	$\lvert E(u_h)\rvert$	I_{eff}	$\lvert J(u) - \tilde{J}(u_h)\rvert$
659	$2.44 \cdot 10^{-05}$	$1.94 \cdot 10^{-05}$	0.79	$5.01 \cdot 10^{-06}$
2467	$2.39 \cdot 10^{-06}$	$1.49 \cdot 10^{-07}$	0.06	$2.24 \cdot 10^{-06}$
9539	$1.33 \cdot 10^{-07}$	$3.26 \cdot 10^{-08}$	0.24	$1.01 \cdot 10^{-07}$
37507	$3.07 \cdot 10^{-09}$	$3.07 \cdot 10^{-09}$	1.00	$5.43 \cdot 10^{-12}$
148739	$9.07 \cdot 10^{-11}$	$1.55 \cdot 10^{-10}$	1.71	$6.47 \cdot 10^{-11}$

Tab. 19: Scenario 3, PD, higher-order interpolation

# DOFs	$\lvert J(u) - J(u_h)\rvert$	$\lvert E(u_h)\rvert$	I_{eff}	$\lvert J(u) - \tilde{J}(u_h)\rvert$
659	$2.44 \cdot 10^{-05}$	$1.51 \cdot 10^{-05}$	0.62	$9.31 \cdot 10^{-06}$
2467	$2.39 \cdot 10^{-06}$	$4.13 \cdot 10^{-07}$	0.17	$2.80 \cdot 10^{-06}$
9539	$1.33 \cdot 10^{-07}$	$1.42 \cdot 10^{-08}$	0.11	$1.19 \cdot 10^{-07}$
37507	$3.07 \cdot 10^{-09}$	$1.62 \cdot 10^{-09}$	0.53	$1.45 \cdot 10^{-09}$
148739	$9.07 \cdot 10^{-11}$	$2.93 \cdot 10^{-11}$	0.32	$6.13 \cdot 10^{-11}$

Tab. 20: Scenario 3, P, block strategy, one update step, $\omega = 0.2$

# DOFs	$\lvert J(u) - J(u_h)\rvert$	$\lvert E(u_h)\rvert$	I_{eff}	$\lvert J(u) - \tilde{J}(u_h)\rvert$
659	$2.44 \cdot 10^{-05}$	$1.71 \cdot 10^{-05}$	0.70	$7.29 \cdot 10^{-06}$
2467	$2.39 \cdot 10^{-06}$	$4.54 \cdot 10^{-07}$	0.19	$2.84 \cdot 10^{-06}$
9539	$1.33 \cdot 10^{-07}$	$1.65 \cdot 10^{-08}$	0.12	$1.17 \cdot 10^{-07}$
37507	$3.07 \cdot 10^{-09}$	$1.88 \cdot 10^{-09}$	0.61	$1.19 \cdot 10^{-09}$
148739	$9.07 \cdot 10^{-11}$	$3.40 \cdot 10^{-11}$	0.37	$5.67 \cdot 10^{-11}$

Tab. 21: Scenario 3, P, block strategy, two update steps, $\omega = 0.2$

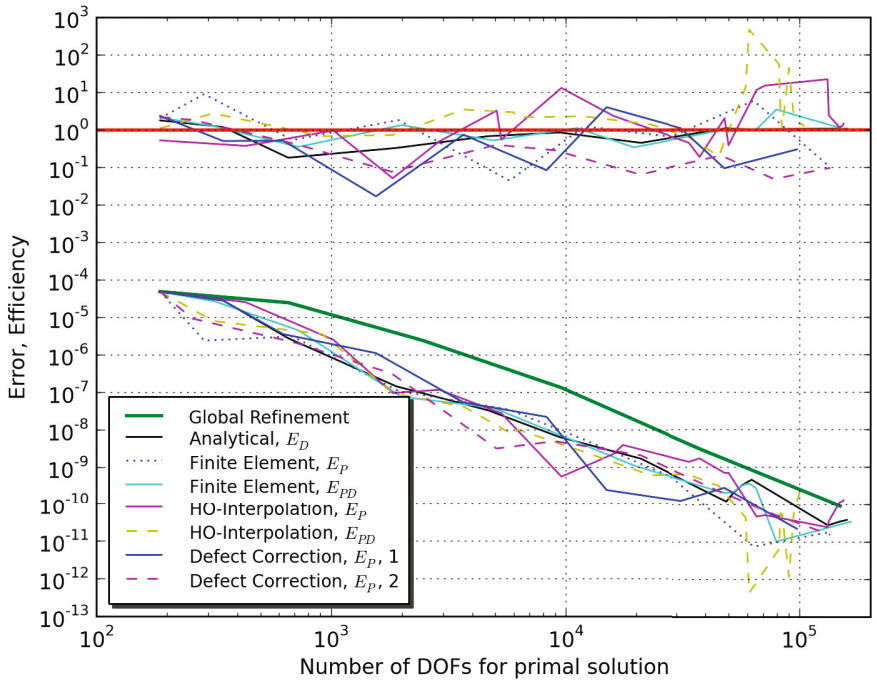

Fig. 13: Error and efficiency plots for scenario 3

5.3.4 Point-value of vorticity

# DOFs	$\lvert J(u) - J(u_h)\rvert$	$\lvert E(u_h)\rvert$	I_{eff}	$\lvert J(u) - \tilde{J}(u_h)\rvert$
2467	$4.04 \cdot 10^{-04}$	$2.29 \cdot 10^{-04}$	0.57	$1.74 \cdot 10^{-04}$
9539	$8.56 \cdot 10^{-05}$	$4.19 \cdot 10^{-05}$	0.49	$4.36 \cdot 10^{-05}$
37507	$1.34 \cdot 10^{-05}$	$8.47 \cdot 10^{-06}$	0.63	$4.91 \cdot 10^{-06}$
148739	$8.18 \cdot 10^{-07}$	$1.87 \cdot 10^{-07}$	0.23	$6.32 \cdot 10^{-07}$

Tab. 22: Scenario 4, D, analytical solution of primal problem, interpolation

# DOFs	$\lvert J(u) - J(u_h)\rvert$	$\lvert E(u_h)\rvert$	I_{eff}	$\lvert J(u) - \tilde{J}(u_h)\rvert$
2467	$4.04 \cdot 10^{-04}$	$1.48 \cdot 10^{-04}$	0.37	$2.56 \cdot 10^{-04}$
9539	$8.56 \cdot 10^{-05}$	$4.34 \cdot 10^{-05}$	0.51	$4.22 \cdot 10^{-05}$
37507	$1.34 \cdot 10^{-05}$	$8.49 \cdot 10^{-06}$	0.63	$4.89 \cdot 10^{-06}$
148739	$8.18 \cdot 10^{-07}$	$1.86 \cdot 10^{-07}$	0.23	$6.32 \cdot 10^{-07}$

Tab. 23: Scenario 4, P, higher-order finite element solution

# DOFs	$\lvert J(u) - J(u_h)\rvert$	$\lvert E(u_h)\rvert$	I_{eff}	$\lvert J(u) - \tilde{J}(u_h)\rvert$
2467	$4.04 \cdot 10^{-04}$	$1.48 \cdot 10^{-04}$	0.37	$2.56 \cdot 10^{-04}$
9539	$8.56 \cdot 10^{-05}$	$4.34 \cdot 10^{-05}$	0.51	$4.22 \cdot 10^{-05}$
37507	$1.34 \cdot 10^{-05}$	$8.49 \cdot 10^{-06}$	0.63	$4.89 \cdot 10^{-06}$
148739	$8.18 \cdot 10^{-07}$	$1.86 \cdot 10^{-07}$	0.23	$6.32 \cdot 10^{-07}$

Tab. 24: Scenario 4, PD, higher-order finite element solution

# DOFs	$\lvert J(u) - J(u_h)\rvert$	$\lvert E(u_h)\rvert$	I_{eff}	$\lvert J(u) - \tilde{J}(u_h)\rvert$
2467	$4.04 \cdot 10^{-04}$	$5.60 \cdot 10^{-04}$	1.39	$9.64 \cdot 10^{-04}$
9539	$8.56 \cdot 10^{-05}$	$7.58 \cdot 10^{-06}$	0.09	$7.80 \cdot 10^{-05}$
37507	$1.34 \cdot 10^{-05}$	$5.22 \cdot 10^{-06}$	0.39	$8.16 \cdot 10^{-06}$
148739	$8.18 \cdot 10^{-07}$	$5.77 \cdot 10^{-07}$	0.71	$1.40 \cdot 10^{-06}$

Tab. 25: Scenario 4, P, higher-order interpolation

# DOFs	$\lvert J(u) - J(u_h)\rvert$	$\lvert E(u_h)\rvert$	I_{eff}	$\lvert J(u) - \tilde{J}(u_h)\rvert$
2467	$4.04 \cdot 10^{-04}$	$3.98 \cdot 10^{-04}$	0.99	$8.02 \cdot 10^{-04}$
9539	$8.56 \cdot 10^{-05}$	$2.70 \cdot 10^{-05}$	0.32	$5.86 \cdot 10^{-05}$
37507	$1.34 \cdot 10^{-05}$	$6.89 \cdot 10^{-06}$	0.51	$6.50 \cdot 10^{-06}$
148739	$8.18 \cdot 10^{-07}$	$1.95 \cdot 10^{-07}$	0.24	$1.01 \cdot 10^{-06}$

Tab. 26: Scenario 4, PD, higher-order interpolation

# DOFs	$\lvert J(u) - J(u_h)\rvert$	$\lvert E(u_h)\rvert$	I_{eff}	$\lvert J(u) - \tilde{J}(u_h)\rvert$
2467	$4.04 \cdot 10^{-04}$	$4.96 \cdot 10^{-04}$	1.23	$8.99 \cdot 10^{-04}$
9539	$8.56 \cdot 10^{-05}$	$5.79 \cdot 10^{-05}$	0.68	$2.77 \cdot 10^{-05}$
37507	$1.34 \cdot 10^{-05}$	$1.34 \cdot 10^{-05}$	1.00	$1.77 \cdot 10^{-08}$
148739	$8.18 \cdot 10^{-07}$	$2.12 \cdot 10^{-07}$	0.26	$1.03 \cdot 10^{-06}$

Tab. 27: Scenario 4, P, block strategy, one update step, $\omega = 0.6$

# DOFs	$\lvert J(u) - J(u_h)\rvert$	$\lvert E(u_h)\rvert$	I_{eff}	$\lvert J(u) - \tilde{J}(u_h)\rvert$
2467	$4.04 \cdot 10^{-04}$	$2.32 \cdot 10^{-04}$	0.57	$1.72 \cdot 10^{-04}$
9539	$8.56 \cdot 10^{-05}$	$1.12 \cdot 10^{-05}$	0.13	$7.44 \cdot 10^{-05}$
37507	$1.34 \cdot 10^{-05}$	$8.65 \cdot 10^{-06}$	0.65	$2.20 \cdot 10^{-05}$
148739	$8.18 \cdot 10^{-07}$	$7.18 \cdot 10^{-07}$	0.88	$1.00 \cdot 10^{-07}$

Tab. 28: Scenario 4, P, block strategy, two update steps, $\omega = 0.6$

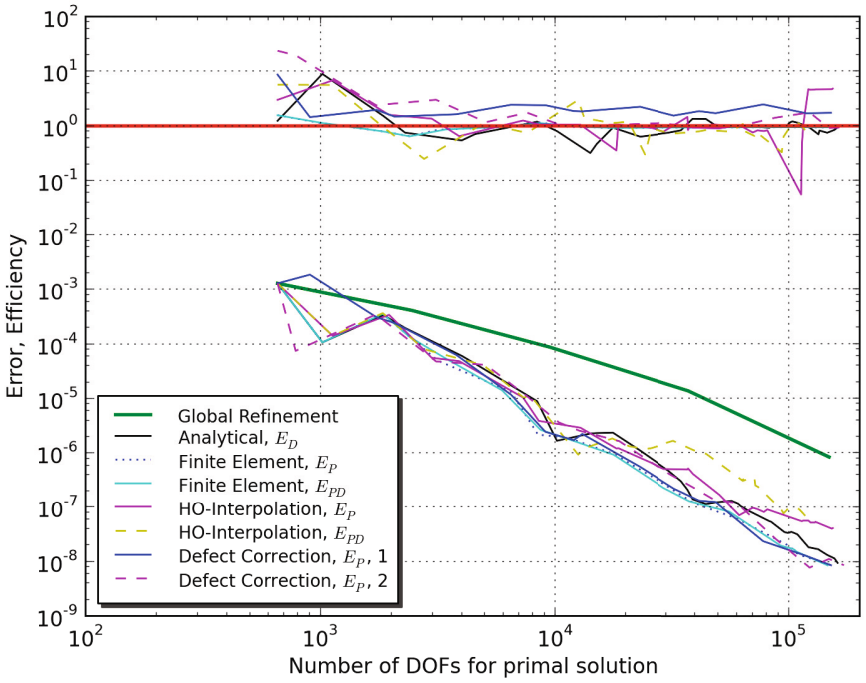

Fig. 14: Error and efficiency plots for scenario 4

5.3.5 Kinetic energy

# DOFs	$\lvert J(u) - J(u_h)\rvert$	$\lvert E(u_h)\rvert$	I_{eff}	$\lvert J(u) - \tilde{J}(u_h)\rvert$
2467	$4.35 \cdot 10^{-03}$	$4.34 \cdot 10^{-03}$	1.00	$1.16 \cdot 10^{-05}$
9539	$2.55 \cdot 10^{-04}$	$2.56 \cdot 10^{-04}$	1.00	$1.17 \cdot 10^{-06}$
37507	$1.55 \cdot 10^{-05}$	$1.56 \cdot 10^{-05}$	1.00	$1.89 \cdot 10^{-08}$
148739	$9.65 \cdot 10^{-07}$	$9.65 \cdot 10^{-07}$	1.00	$2.94 \cdot 10^{-10}$

Tab. 29: Scenario 5, D, analytical solution of primal problem, interpolation

# DOFs	$\lvert J(u) - J(u_h)\rvert$	$\lvert E(u_h)\rvert$	I_{eff}	$\lvert J(u) - \tilde{J}(u_h)\rvert$
2467	$4.35 \cdot 10^{-03}$	$4.17 \cdot 10^{-03}$	0.96	$1.83 \cdot 10^{-04}$
9539	$2.55 \cdot 10^{-04}$	$2.52 \cdot 10^{-04}$	0.99	$2.98 \cdot 10^{-06}$
37507	$1.55 \cdot 10^{-05}$	$1.55 \cdot 10^{-05}$	1.00	$5.01 \cdot 10^{-08}$
148739	$9.65 \cdot 10^{-07}$	$9.64 \cdot 10^{-07}$	1.00	$8.03 \cdot 10^{-10}$

Tab. 30: Scenario 5, P, higher-order finite element solution

# DOFs	$\lvert J(u) - J(u_h)\rvert$	$\lvert E(u_h)\rvert$	I_{eff}	$\lvert J(u) - \tilde{J}(u_h)\rvert$
2467	$4.35 \cdot 10^{-03}$	$4.17 \cdot 10^{-03}$	0.96	$1.83 \cdot 10^{-04}$
9539	$2.55 \cdot 10^{-04}$	$2.52 \cdot 10^{-04}$	0.99	$2.98 \cdot 10^{-06}$
37507	$1.55 \cdot 10^{-05}$	$1.55 \cdot 10^{-05}$	1.00	$5.01 \cdot 10^{-08}$
148739	$9.65 \cdot 10^{-07}$	$9.64 \cdot 10^{-07}$	1.00	$8.03 \cdot 10^{-10}$

Tab. 31: Scenario 5, PD, higher-order finite element solution

# DOFs	$\lvert J(u) - J(u_h)\rvert$	$\lvert E(u_h)\rvert$	I_{eff}	$\lvert J(u) - \tilde{J}(u_h)\rvert$
2467	$4.35 \cdot 10^{-03}$	$3.57 \cdot 10^{-03}$	0.82	$7.81 \cdot 10^{-04}$
9539	$2.55 \cdot 10^{-04}$	$2.52 \cdot 10^{-04}$	0.99	$3.03 \cdot 10^{-06}$
37507	$1.55 \cdot 10^{-05}$	$1.57 \cdot 10^{-05}$	1.01	$1.23 \cdot 10^{-07}$
148739	$9.65 \cdot 10^{-07}$	$9.67 \cdot 10^{-07}$	1.00	$2.07 \cdot 10^{-09}$

Tab. 32: Scenario 5, P, higher-order interpolation

# DOFs	$\lvert J(u) - J(u_h)\rvert$	$\lvert E(u_h)\rvert$	I_{eff}	$\lvert J(u) - \tilde{J}(u_h)\rvert$
2467	$4.35 \cdot 10^{-03}$	$3.35 \cdot 10^{-03}$	0.77	$1.01 \cdot 10^{-03}$
9539	$2.55 \cdot 10^{-04}$	$2.51 \cdot 10^{-04}$	0.98	$4.25 \cdot 10^{-06}$
37507	$1.55 \cdot 10^{-05}$	$1.56 \cdot 10^{-05}$	1.01	$1.01 \cdot 10^{-07}$
148739	$9.65 \cdot 10^{-07}$	$9.67 \cdot 10^{-07}$	1.00	$1.72 \cdot 10^{-09}$

Tab. 33: Scenario 5, PD, higher-order interpolation

# DOFs	$\lvert J(u) - J(u_h)\rvert$	$\lvert E(u_h)\rvert$	I_{eff}	$\lvert J(u) - \tilde{J}(u_h)\rvert$
2467	$4.35 \cdot 10^{-03}$	$4.67 \cdot 10^{-03}$	1.07	$3.16 \cdot 10^{-04}$
9539	$2.55 \cdot 10^{-04}$	$3.03 \cdot 10^{-04}$	1.19	$4.77 \cdot 10^{-05}$
37507	$1.55 \cdot 10^{-05}$	$1.92 \cdot 10^{-05}$	1.23	$3.63 \cdot 10^{-06}$
148739	$9.65 \cdot 10^{-07}$	$1.20 \cdot 10^{-06}$	1.24	$2.36 \cdot 10^{-07}$

Tab. 34: Scenario 5, P, block strategy, one update step, $\omega = 0.7$

# DOFs	$\lvert J(u) - J(u_h)\rvert$	$\lvert E(u_h)\rvert$	I_{eff}	$\lvert J(u) - \tilde{J}(u_h)\rvert$
2467	$4.35 \cdot 10^{-03}$	$5.26 \cdot 10^{-03}$	1.21	$9.61 \cdot 10^{-03}$
9539	$2.55 \cdot 10^{-04}$	$3.01 \cdot 10^{-04}$	1.18	$5.57 \cdot 10^{-04}$
37507	$1.55 \cdot 10^{-05}$	$1.83 \cdot 10^{-05}$	1.18	$3.39 \cdot 10^{-05}$
148739	$9.65 \cdot 10^{-07}$	$1.14 \cdot 10^{-06}$	1.18	$2.10 \cdot 10^{-06}$

Tab. 35: Scenario 5, P, block strategy, two update steps, $\omega = 0.7$

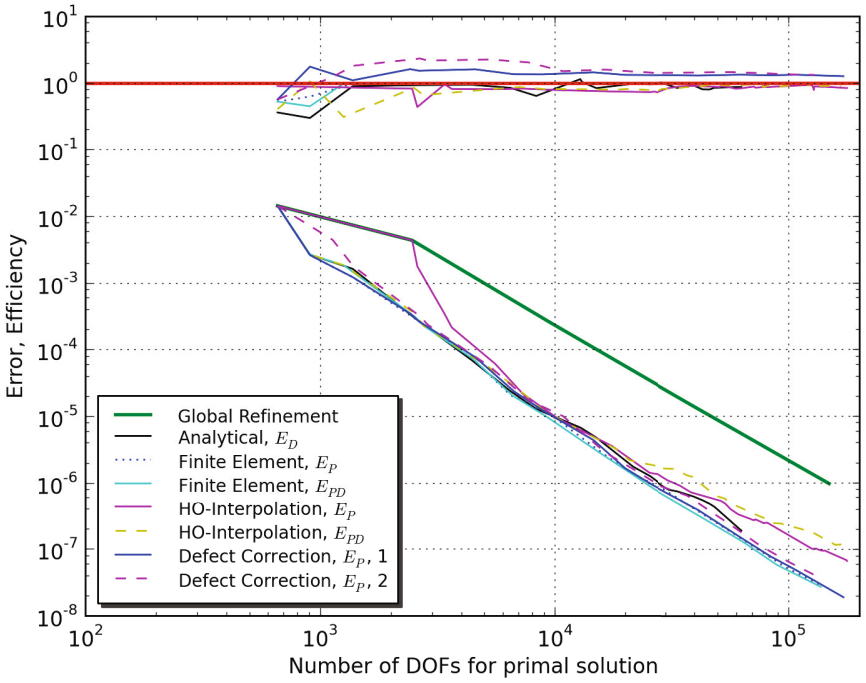

Fig. 15: Error and efficiency plots for scenario 5

5.4 Summary of results

Based on the presented numerical results, the performance of different variants of the error estimator can be quantified with respect to the efficiency of the error estimators evaluated on uniform and locally refined meshes. For this purpose, the mean relative deviation (MRD) of the efficiency indicator is introduced to investigate the difference between the estimated error and

	D anal.	P ho-fe	PD ho-fe	P ho-int	PD ho-int	P block, 1	P block, 2
Scenario 1	0.75	0.76	0.75	2.76	7.22	3.30	2.47
Scenario 2	0.00	0.40	0.11	0.47	0.18	2.20	1.76
Scenario 3	1.02	1.18	1.07	1.74	3.82	3.35	2.81
Scenario 4	1.44	1.67	1.67	3.17	1.58	0.89	2.02
Scenario 5	0.00	0.01	0.01	0.06	0.08	0.19	0.19
Avg.	**0.64**	**0.8**	**0.72**	**1.64**	**2.58**	**1.99**	**1.85**

Tab. 36: Mean relative deviation, global refinement

	D anal.	P ho-fe	PD ho-fe	P ho-int	PD ho-int	P block, 1	P block, 2
Scenario 1	0.77	1.82	29.35	13.24	15.31	4.66	7.19
Scenario 2	0.00	3.91	28.81	1.57	1.14	8.64	5.91
Scenario 3	0.66	5.15	0.58	4.56	26.94	8.88	6.74
Scenario 4	0.51	0.18	0.17	1.74	0.84	1.26	2.72
Scenario 5	0.34	0.11	0.15	0.21	0.24	0.41	0.65
Avg.	**0.46**	**2.23**	**11.81**	**4.26**	**8.89**	**4.77**	**4.64**

Tab. 37: Mean relative deviation, local refinement

the real error in J:

$$MRD := \frac{1}{N}\sum_{i=1}^{N} I_{\text{rel}}(i), \quad I_{\text{rel}} := \frac{|1 - I_{\text{eff}}|}{\min(1, I_{\text{eff}})}.$$

The two tables contain the averaged MRD values of sequences of simulations for each scenario based on uniform meshes (Tab. 36) and locally refined meshes (Tab. 37). It can be seen that the error estimator variant that makes use of the analytical solution of the primal problem has the lowest MRD. Although this variant cannot be used for general applications since the exact solution is unknown, it can serve as a reference for the current investigation. The ordering of the evaluation strategies with respect to the averaged MRD values roughly reflects the computational costs associated with the evaluation of the error estimators. The estimators that make use of higher-order finite element solutions are the most efficient ones, but are computationally expensive. The estimators based on higher-order interpolation show higher MRD but are comparably cheap to compute. The block strategy leads to estimators that have MRD in between those of the aforementioned strategies.

The economy of the adaptive methods can be quantified in terms of the ratio of error in J and number of unknowns of the discrete system. In the error plots it can be seen that except for scenario 2 the error estimators lead to economic meshes on which the evaluated values that are of interest could be approximated better compared to solutions on uniform meshes with the same number of degrees of freedom. Although the strategies based on higher-order interpolation showed good properties, it can be observed that the block strategy leads to more economical meshes for the considered scenarios.

The improved goal value $\tilde{J}(u_h)$, see Equation (7), is a better approximation of the exact value $J(u)$ than the canonical approximation $J(u_h)$ for the majority of the performed numerical simulations. The error $|\tilde{J}(u_h) - J(u)|$ is up to one order of magnitude lower than $|J(u_h) - J(u)|$ for most cases, and for scenarios 2 and 5, the enhancement is significantly higher. Hence, the so-called improved goal value is actually an improvement in this investigation.

6 Conclusion

We investigated different strategies for approximating the exact solutions of the primal and dual problem in the context of a posteriori error estimators for certain goal functionals. Several variants of a posteriori error representations and local error indicators have been presented and in particular, we have proposed a new block strategy based on the solution of cell-wise Dirichlet problems, nested in a global defect-correction iteration. The strategies have been compared in a systematical way for five scenarios with different goal functionals and analytically known exact solutions. The efficiency of the error estimators has been analyzed for uniformly and locally refined meshes and the economy of the unterlying adaptive methods has been evaluated. In four of the five scenarios the adaptive methods lead to optimized meshes on which the quantity of interest could be approximated with a significantly smaller number of unknowns than on the uniform meshes. The computational costs of the different strategies reflected roughly the quality in the sense of efficiency of the estimator and the economy of the adaptive method. The block strategy offers the ability to control the quality of the approximation and the computational effort by changing the number of iterations, and furthermore has good parallelization properties. Similar approaches bases on the solution of local Neumann problems should be investigated in the future.

In many applications of environmental sciences, the underlying phenomena have a time-varying structure that can be modelled by instationary PDEs. In such situations goal oriented error estimators and mesh adaptation strategies can be very costly, as the dual problem is also time-dependent and posed backwards in time. Efficient calculation of error estimates and local indicators for temporal and spatial mesh adaptation in this context is challenging, but can help to understand complex physical processes that can hardly be modelled and calculated using today's high-performance computers.

Acknowledgments

The authors acknowledge support from DFG priority programme SPP-1276 MetStröm: Multiple Scales in Fluid Mechanics and Meteorology.

References

[AAB+10] H. Anzt, W. Augustin, M. Baumann, H. Bockelmann, T. Gengenbach, T. Hahn, V. Heuveline, E. Ketelaer, D. Lukarski, A. Otzen, S. Ritterbusch, B. Rocker, S. Ronnas, M. Schick, C. Subramanian, J.-P. Weiss, and F. Wilhelm. HiFlow3 – A Flexible and Hardware-Aware Parallel Finite Element Package. EMCL Preprint Series, 2010.

[AO00] Mark Ainsworth and J. Tinsley Oden. *A Posteriori Error Estimation in Finite Element Analysis*. John Wiley & Sons Inc., 2000.

[BE03] M. Braack and A. Ern. A posteriori control of modeling errors and discretization errors. *Multiscale Model. Simul.*, 1(2):221–238, 2003.

[BEG03] Erik Burman, Alexandre Ern, and Vincent Giovangigli. An adaptive finite element method with crosswind diffusion for low Mach, steady, laminar combustion. *J. Comput. Phys.*, 188:472–492, July 2003.

[BF91] Franco Brezzi and Richard S. Falk. Stability of Higher-Order Hood-Taylor Methods. *SIAM Journal on Numerical Analysis*, 28(3):581–590, 1991.

[BH06] S. Bönisch and V. Heuveline. Advanced Flow Visualization with Hivision. In R. et al. Rannacher, editor, *Reactive Flows, Diffusion and Transport*. Springer, Berlin, 2006.

[BHR02] R. Becker, V. Heuveline, and R. Rannacher. An Optimal Control Approach to Adaptivity in Computational Fluid Mechanics. *International Journal for Numerical Methods in Fluids*, 40(1-2):105–120, 2002.

[BR99] Malte Braack and Rolf Rannacher. Adaptive Finite Element Methods for Low-Mach-Number Flows with Chemical Reactions. In *of 30th Computational Fluid Dynamics, von Karman Institute*, pages 1–93, 1999.

[BR03] Wolfgang Bangerth and Rolf Rannacher. *Adaptive Finite Element Methods for Differential Equations*. Birkhäuser Verlag, 2003.

[BR06] M. Braack and T. Richter. Solutions of 3D Navier-Stokes benchmark problems with adaptive finite elements. *Computers & Fluids*, 35(4):372 – 392, 2006.

[Bre74] Franco Brezzi. On the existence, uniqueness, and approximation of saddle point problems arising from Lagrangian multipliers. *Revue française d'automatique, informatique, recherche opérationnelle. Analyse Numérique*, 8(2):129–151, 1974.

[BW85] Randolph E. Bank and Alan Weiser. Some a posteriori error estimators for elliptic partial differential equations. *Math. Comp*, 44:283–301, 1985.

[CH08] Jaime Carpio Huertas. *Duality methods for time-space adaptivity to calculate the numerical solution of partial differential equations*. PhD thesis, Matemática Aplicada a la Ingeniería Industrial / E.T.S.I. Industriales (UPM), 2008.

[Cho68] A.J. Chorin. Numerical solution for the Navier-Stokes equations. *Math. Comp*, 22:745–762, 1968.

[EEHJ95] Kenneth Eriksson, Don Estep, Peter Hansbo, and Claes Johnson. Introduction to Adaptive Methods for Differential Equations. *Acta Numerica*, 4(-1):105–158, 1995.

[Gal98] G. P. Galdi. *An Introduction to the Mathematical Theory of the Navier–Stokes Equations*, volume 1: Linearized Steady Problems. Springer, 1998.

[Har08] Ralf Hartmann. Multitarget error estimation and adaptivity in aerodynamic flow simulations. *SIAM J. Sci. Comput.*, 31(1):708–731, 2008.

[HR03] V. Heuveline and R. Rannacher. Duality-Based Adaptivity in the hp-Finite Element Method. *Journal of Numerical Mathematics*, 11(2):95–113, 2003.

[HR06] V. Heuveline and R. Rannacher. Adaptive FEM for Eigenvalue Problems with Application in Hydrodynamic Stability Analysis. *Journal of Numerical Mathematics*, pages 1–32, 2006.

[HS07] V. Heuveline and F. Schieweck. On the Inf-Sup Condition for Higher Order Mixed FEM on Meshes with Hanging Nodes. *Mathematical Modelling and Numerical Analysis M2AN*, 41(1):1–20, 2007.

[HW06] V. Heuveline and A. Walther. Online Checkpointing for Parallel Adjoint Computation in PDEs: Application to Goal-Oriented Adaptivity and Flow Control. In W. et al. Nagel, editor, *Proceedings of Euro-Par 2006*, volume 4128 of *LNCS*, pages 689–699. Springer, 2006.

[MGH+05] Michael B. Monagan, Keith O. Geddes, K. Michael Heal, George Labahn, Stefan M. Vorkoetter, James McCarron, and Paul DeMarco. *Maple 10 Programming Guide*. Maplesoft, Waterloo ON, Canada, 2005.

[Sch00] F. Schieweck. A General Transfer Operator for Arbitrary Finite Element Spaces. Preprint 25/00, University Magdeburg, 2000.

[SJJ11] L. Scheck, S. C. Jones, and M. Juckes. The Resonant Interaction of a Tropical Cyclone and a Tropopause Front in a Barotropic Model, Part I: Zonally-oriented Front. *J. Atmos. Sci.*, 68(3):405–419, 2011.

[Ste03] Ekkehard Stein, Erwin [Hrsg.]; Ramm, editor. *Error controlled adaptive finite elements in solid mechanics*. Wiley, Chichester, 2003.

[SV07] Michael Schmich and Boris Vexler. Adaptivity with Dynamic Meshes for Space-Time Finite Element Discretizations of Parabolic Equations. *SIAM J. Sci. Comput.*, 30(1):369–393, 2007.

[Ver96] Rüdiger Verfürth. *A Review of A Posteriori Error Estimation and Adaptive Mesh-Refinement Techniques*. Wiley-Teubner, 1996.

Preprint Series of the Engineering Mathematics and Computing Lab

recent issues

No. 2010-04 Hartwig Anzt, Tobias Hahn, Vincent Heuveline, Björn Rocker: GPU Accelerated Scientific Computing: Evaluation of the NVIDIA Fermi Architecture; Elementary Kernels and Linear Solvers

No. 2010-03 Hartwig Anzt, Vincent Heuveline, Björn Rocker: Energy Efficiency of Mixed Precision Iterative Refinement Methods using Hybrid Hardware Platforms: An Evaluation of different Solver and Hardware Configurations

No. 2010-02 Hartwig Anzt, Vincent Heuveline, Björn Rocker: Mixed Precision Error Correction Methods for Linear Systems: Convergence Analysis based on Krylov Subspace Methods

No. 2010-01 Hartwig Anzt, Vincent Heuveline, Björn Rocker: An Error Correction Solver for Linear Systems: Evaluation of Mixed Precision Implementations

No. 2009-02 Rainer Buchty, Vincent Heuveline, Wolfgang Karl, Jan-Philipp Weiß: A Survey on Hardware-aware and Heterogeneous Computing on Multicore Processors and Accelerators

No. 2009-01 Vincent Heuveline, Björn Rocker, Staffan Ronnas: Numerical Simulation on the SiCortex Supercomputer Platform: a Preliminary Evaluation